DEVELOPMENT OF AN INTEGRATED SYSTEM FOR FLOW VISUALIZATION IN AIR USING NEUTRALLY-BUOYANT BUBBLES

R. W. Hale, et al

Sage Action, Incorporated

Prepared for:

Office of Naval Research

December 1971

AD 756691

SAI-RR 7107
December 1971

DEVELOPMENT OF AN INTEGRATED SYSTEM FOR FLOW VISUALIZATION IN AIR USING NEUTRALLY-BUOYANT BUBBLES

by

R. W. Hale, P. Tan, R. C. Stowell and D. E. Ordway

SAGE ACTION, Inc.
Ithaca, New York

Sponsored by:

Aeronautics, Code 461
Naval Applications Group
Office of Naval Research
Arlington, Virginia 22217

Prepared under Contract N00014-68-C-0434
NR 212-186

UNCLASSIFIED

Security Classification

DOCUMENT CONTROL DATA - R & D

(Security classification of title, body of abstract and indexing annotation must be entered when the overall report is classified)

ORIGINATING ACTIVITY (Corporate author) SAGE ACTION, Inc. P. O. Box 416 Ithaca, New York 14850	2a. REPORT SECURITY CLASSIFICATION Unclassified 2b. GROUP

3. REPORT TITLE

DEVELOPMENT OF AN INTEGRATED SYSTEM FOR FLOW VISUALIZATION IN AIR USING NEUTRALLY-BUOYANT BUBBLES

4. DESCRIPTIVE NOTES (Type of report and inclusive dates)

Technical Report #2, 1 February 1969 - 30 June 1971

5. AUTHOR(S) (First name, middle initial, last name)

R. W. Hale, P. Tan, R. C. Stowell and D. E. Ordway

6. REPORT DATE	7a. TOTAL NO OF PAGES	7b. NO OF REFS
December 1971	~~66~~ 69	22

8a. CONTRACT OR GRANT NO	9a. ORIGINATOR'S REPORT NUMBER(S)
N00014-68-C-0434 b. PROJECT NO	SAI-RR 7107
c. d.	9b. OTHER REPORT NO(S) (Any other numbers that may be assigned this report)

10. DISTRIBUTION STATEMENT

Approved for public release; distribution unlimited.

11. SUPPLEMENTARY NOTES	12. SPONSORING MILITARY ACTIVITY
Details of illustrations in this document may be better studied on microfiche.	Aeronautics, Code 461 Office of Naval Research Arlington, Virginia 22217

13. ABSTRACT

A new technique for flow visualization in air is presented. This technique employs small, neutrally-buoyant bubbles to map out particle paths and measure velocities, even in turbulent aerodynamic flows. An integrated visualization system was developed, comprised of a unique means to generate the bubbles, a compact illumination unit and specialized photography. This is described in detail, together with the setup and application of the system. Three test programs were carried out in conventional subsonic wind tunnels to assess and improve the system performance. These tests are discussed and an evaluation is given of the system's current capabilities, accuracy and utility. A number of photographs illustrate the various facets of the technique.

DD FORM 1 NOV 65 1473 (PAGE 1)

0101-807-6801

I-a

UNCLASSIFIED

Security Classification

KEY WORDS	LINK A		LINK B		LINK C	
	ROLE	WT	ROLE	WT	ROLE	WT
Flow visualization						
Neutrally-buoyant bubbles						
Bubble generator						
Aerodynamic testing						
Wind tunnel tests						
Streamlines						
Particle paths						
Turbulent flow						
Illumination						
Photography						
Light modulation						
Flow tracing accuracy						
Tip vortex						

FOREWORD

This work was performed for the Office of Naval Research, Aeronautics, Code 461, under ONR Contract N00014-68-C-0434. The research reported was carried out by SAGE ACTION, Inc. over the period from 1 February 1969 to 30 June 1971. T. L. Wilson and D. C. Lauver of the ONR served as technical monitors.

The authors would like to acknowledge the cooperation and assistance afforded us during our three wind tunnel test programs. We are particularly grateful to R. L. Wardlaw and his Staff at the National Aeronautical Establishment, R. P. White, Jr. and J. C. Balcerak of Rochester Applied Science Associates, and S. M. Gottlieb and his Staff at the Naval Ship Research and Development Center.

TABLE OF CONTENTS

INTRODUCTION

Ever since man has been aware of the many ways air movement affects and even controls his life, he has longed to see it. Nature has provided us with swirling snow and floating seed pods that reveal, often dramatically, the wind motion. But man, over the years, has really had little success in improving very much on this natural flow visualization. The birth of aeronautics gave new impetus to this search, though, and various techniques have been tried since, especially within the controlled environment of the wind tunnel.

Without much question, the most popular flow tracer employed to date has been smoke. Some outstanding work has been done with smoke that has led to significant discoveries. Unfortunately, though, there are certain limitations to this technique. Smoke particles are very small, typically less than a micron in diameter. From this property they derive their ability to follow air motion faithfully. On the other hand, they cannot be viewed or photographed individually. As a result, we must create a relatively dense cloud of particles and view the motion of the edges of this cloud rather than the particles themselves. This alone presents difficulties sometimes. Even worse, the cloud will diffuse if the air motion is turbulent, the edges first becoming indistinct and then disappearing as the particle concentration drops. Consequently, the best flow visualization with smoke has been carried out in special, very low turbulence, "smoke" tunnels.

To provide flow visualization in conventional tunnels with modest turbulence levels and with aircraft configurations, for example, which introduce even higher turbulence levels, a different approach is needed. Namely, we must be able to follow the path of individual particles. For accuracy with larger particles, however, they must be much lighter. The soap bubble is an ideal particle, extremely light yet fairly rigid. In fact, a bubble can be made even neutrally buoyant in air by filling it with a light gas.

In 1967, we devised a unique means to generate large numbers of helium-filled bubbles, about 1/8" in diameter, in a rapid, continuous fashion. This device was initially employed with remarkable success to visualize the motion of the wind through a field of crops. The bubbles proved to be surprisingly durable and appeared to follow severe fluctuations in wind velocity and direction with considerable accuracy. After these experiments, the bubble generating device, or head, was improved and a console developed for supplying the necessary constituents of soap, helium and air at the proper flow rates.

Since 1968, most of our attention has been focused on flow visualization in wind tunnels at higher airspeeds. The early part of this work is reported in Ref. 1. Our main objective was to gain a better understanding of the operation

of the original low-speed head as a two-phase flow device. Principally, we learned how the flow rates of the three constituents control the bubble size, density and generation rate. Based on this information, we then designed and tested a prototype high-speed head for implanting bubbles in airstreams with velocities as high as 200 fps.

Although we did not achieve bubble formation at airspeeds this high, we were greatly encouraged by the results and felt that the feasibility of the technique was proven. The tests indicated the need to develop a better head design and soap solution, as well as better methods of lighting and photography. At the same time, we could see no inherent limitation in going to higher airspeeds.

Perhaps more important, we saw for the first time the true potential of this flow visualization technique in wind tunnel testing. Without question, the most impressive sight was the bubble motion within the separation region above a two-dimensional airfoil at high angle of attack. This was a completely new experience. The bubbles traced out torturous paths, each different but displaying a surprising amount of spanwise movement. It soon became evident that unraveling an unsteady, turbulent flow is a much more difficult task than analyzing the traditional laminar streamline patterns we have become accustomed to seeing. If the bubbles can really describe such complex behavior, we must be prepared to work harder to understand what they are telling us.

This investigation laid the foundation for the present investigation. The overall objectives were threefold. First, we wanted to be able to implant bubbles at still higher airspeeds. This called for further head development, together with some experimentation on bubble film solutions. Second, it was essential to assemble the various elements into an integrated flow visualization system. This included a substantial effort on lighting and photographic techniques also. Foremost in our considerations, we felt the system had to be practical and economical, avoiding any special wind tunnel arrangements. Third, a series of wind tunnel tests were needed to assess the performance of the system, particularly with regard to accuracy, adaptability and utility. These objectives were accomplished and the system now stands as a working tool with established capabilities. There are some limitations, of course, but these appear to be due only to the current state of development of the elements that make up the system.

In *Section 1*, a brief historical background is presented, followed by a general description of the flow visualization system together with representative photographs from the wind tunnel tests. Details of the tests themselves and the specific test objectives are covered in *Section 2*. The development of each system element is then discussed in *Section 3*. Finally, a thorough evaluation of both the technique and the system is given in *Section 4*. *Conclusions And*

Recommendations complete the report, summarizing the state-of-the-art as it has been advanced to this point. Effort has been made throughout to make the documentation as comprehensive as possible.

1 THE ONR/SAI AIR FLOW VISUALIZATION SYSTEM

1.1 Historical Background

There is evidence of interest in bubbles as early as Roman times. But not until the late 17th century did a scientific interest develop in soap bubbles and soap films as a means to study basic physical phenomena. Robert Hooke, and later Isaac Newton, used them in developing the theory of optics. Subsequently, in the 19th century, Joseph Plateau and J. W. Gibbs studied capillary forces by means of soap films and bubbles. Films have been applied more recently to solve minimal area problems and differential equations with complicated boundary conditions. Even today, soap films are helping the investigation of a number of problems in surface and colloid chemistry[2].

Probably the most extensive treatise on soap bubbles is a series of lectures given by C. V. Boys at the turn of this century[3]. He describes many fascinating experiments with both bubbles and films. More recently, A. L. Kuehner[4,5] experimented with various film solutions to make long-lived bubbles. A. V. Grosse[6], in turn, formulated a new solution based partly on Kuehner's work and performed a series of experiments in the same spirit as Boys.

So far, we have found no record of soap bubbles as aerodynamic flow tracers until well after the birth of aviation. C. N. H. Lock[7], in 1928, mentioned some work on bubbles by his colleague, H. C. H. Townend, at the NPL in England. Townend apparently built an apparatus to produce a steady stream of bubbles filled with coal gas, to make them roughly neutrally buoyant. According to Lock, he applied his technique to a study of a propeller flowfield, but we have not been able to uncover any record of this work yet, or a description of his apparatus.

Eight years later, M. H. Redon and M. F. Vinsonneau[8] published a paper describing a device for generation of small bubbles in a wind tunnel and showing a set of streak photographs. This work was done at the Institute for Fluid Mechanics in Marseille, France. In the same year, Redon applied for a U. S. Patent[9]. A drawing of his basic design is reproduced in Fig. 1.

His design employs a continuous flow rate of the constituents, as in our design, rather than blowing the bubbles off a ring, as in the so-called "dip-and-blow" methods. With a solution of 5% Marseille soap in distilled water, he achieved bubble production rates of 20 to 60 bubbles per second at tunnel speeds up to about 100 fps. The bubbles were filled with air, but he experimented with hydrogen as well. By emitting smoke and bubbles simultaneously and comparing "some characteristic flow patterns presenting strong deflections", he concluded that the bubbles filled with air were satisfactory and

gave the same trajectories.

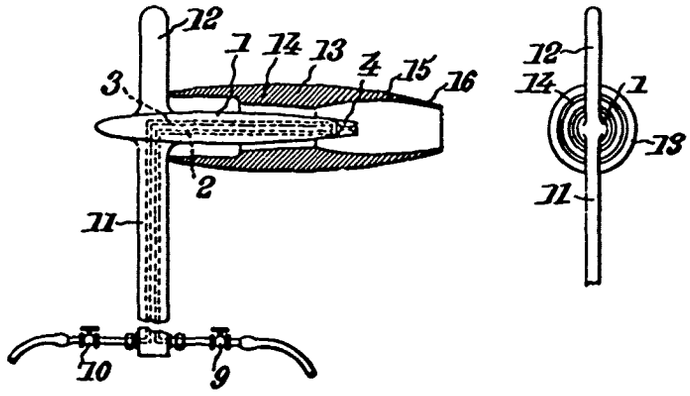

Figure 1. Redon's Bubble Generator (1936)

Although Redon's device seemed to work well and his streak photographs are good, we can find no later reference to it directly. J. Kampé de Fériet[10], however, at the Fifth International Congress for Applied Mechanics in 1938, reported some statistical measurements of turbulence made with bubbles in a wind tunnel. This was done at the Institute for Fluid Mechanics in Lille, France. There was no information on how tne bubbles were produced, but we suspect it may have been with Redon's device.

Since that time, we have found no effort on visualization in air with bubbles until the last ten years. In 1961, B. V. Johnson[11] generated small bubbles with a concentric arrangement of two fine tubes and examined the flow within a cylindrical vortex tube. Using a light and chopper wheel, he also determined rotational velocities. From this beginning, but without knowledge of Redon's accomplishments, we began our own development of the technique in 1967.

1.2 General Description Of Setup

The three principal elements of the air flow visualization system are (i) the bubble generator itself, (ii) the lamp, together with its associated optics and electronics for illuminating the bubbles and (iii) the photographic equipment to record the bubble paths. The general arrangement of these elements for the wind tunnel tests is shown schematically in Fig. 2.

The bubble generator consists of the head, in which the bubbles are actually formed, and a console that supplies the constituents to the head. Only the

Figure 2. General Arrangement Of ONR/SAI Air Flow Visualization System

1 HEAD
2 BUBBLE GENERATOR CONSOLE
3 ARC LAMP OPTICAL SHROUD
4 MODULATOR
5 POWER SUPPLY

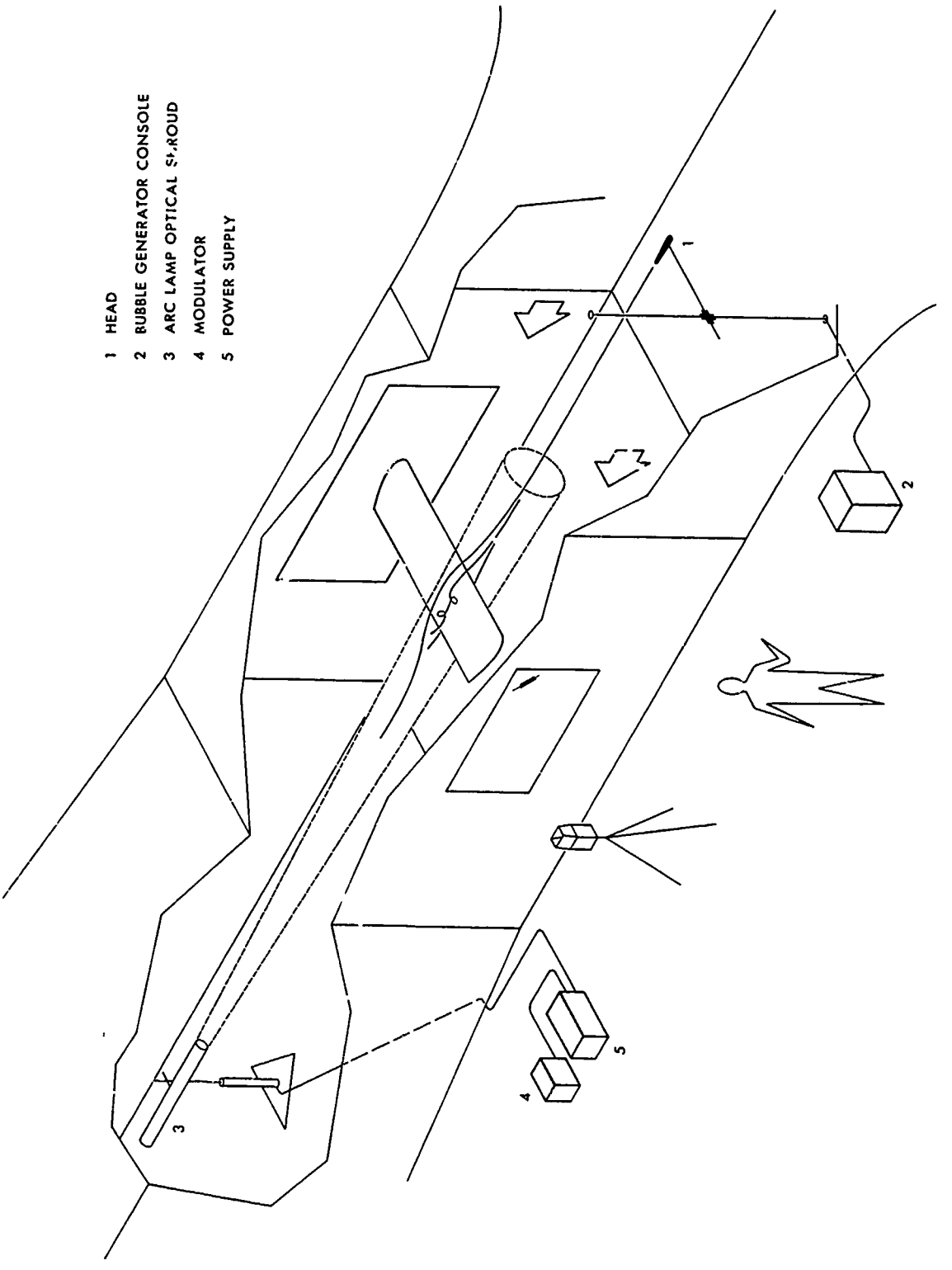

head is situated in the tunnel. It is located far enough upstream of the aerodynamic model to avoid any disturbance to the flow pattern under study. The head currently employed is 5/8" in diameter and approximately 4 1/2" long with a 3/8" diameter stem perpendicular to the main body. Compressed air is supplied to the head through this stem, while helium and bubble film solution are introduced through smaller tubes directly upstream of the stem. The most convenient mounting, as illustrated, is to clamp the stem to a vertical rod which spans the test section off to one side. In this way, the position of the head, and therefore the point where the bubbles enter the flow, can easily be adjusted within the tunnel cross section.

The details of how the bubbles are formed within the head will be described later. After formation, the bubbles are injected into the surrounding freestream and reach the freestream velocity quickly within a short distance. They are then carried by the airstream through the flow pattern under study and downstream into the tunnel diffuser. Some bubbles are so durable they even pass around the entire tunnel circuit and through the test section a second time, including traversal of the tunnel fan and screens!

The bubbles emerge from the head at a fairly even rate. We estimate from our photographs that this bubble production rate R is as high as 500 bubbles per second (bps), or perhaps even higher. If we picture the bubbles following a single streamline, one behind the other, at a stream velocity V (fps), the spacing between bubbles is V/R (ft). For example, if R = 500 bps and V = 100 fps, we have a spacing of 0.2' or 2.4".

The normal wind tunnel turbulence, however, also spreads the bubbles out laterally as they are carried downstream. Typically, we find that about 10' downstream of the head the bubbles can pass anywhere through a circle on the order of 5" in diameter. This natural dispersion is quite desirable, though, since only a single head is needed to visualize a flow pattern whose spanwise extent is of this size. Otherwise more heads are required.

The bubble generator console is set at a convenient location outside the tunnel. Three lengths of plastic tubing carry the compressed air, helium and bubble film solution from the console through the tunnel wall to the head. These tubes are thin and flexible and usually fit through some existing holes in the tunnel. The console contains micro-metering valves to control the constituent flowrates, a pressurized cylinder to hold the bubble film solution, and inlet connections for high-pressure air and helium. If the console is close to a tunnel window, the bubble size, density and production rate can be observed and adjusted simultaneously.

Turning now to illumination, we have employed a high-intensity xenon arc lamp to light the bubbles. This lamp has a very narrow beam, about 8° included

angle, but the intensity distribution across the beam is characteristically Gaussian rather than uniform. To achieve a uniform distribution, we have placed the lamp in an optical shroud containing a pair of condensing lenses, an iris and a projection lens. These elements are arranged in a fashion similar to a conventional slide projector. With this shroud, we can vary the beam angle and focus the uniform field of the light throughout the region of the flow under investigation.

The optical shroud is generally located inside the tunnel, downstream in the tunnel diffuser as shown in Fig. 2. The reason for this is to provide as much contrast as possible between the illuminated bubbles and the background. Maximum contrast is essential for photography because the bubbles reflect so little of the light that falls on them. With the beam directed upstream, virtually no light falls on the walls, floor or ceiling of the test section so they remain dark even if they are not painted black. As a result, we can photograph from any direction normal to this beam and have a dark background. The effect is similar to viewing the light beam from a projector in a darkened room. That is, any specks of dust within the beam are clearly visible, though they could not be seen readily otherwise.

We do get some light scattered from the model onto the tunnel walls, but this is minimized by painting the model black. The interior tunnel lights should, of course, be turned off. It is helpful, too, to block out most of the light from the outside. Based upon our work to date, we feel that this lighting scheme is the best one for testing in current subsonic tunnels.

A power supply and a modulator complete the lighting part of the system. These units are usually outside the tunnel with a single power lead running from the power supply to the arc lamp. The power supply is made by the arc lamp manufacturer and has a high-voltage starting circuit. The modulator, on the other hand, is an electronic device we designed and built to reduce the lamp brightness intermittently at precise intervals. Consequently, the bubble paths appear "dashed" or broken rather than continuous. From the measured length between breaks in the streak and the known time interval, the actual bubble velocity can be found. For the present design the modulation frequency can be varied from about 100 to 10,000 Hz. The unit is connected directly to the power supply with an output to an oscilloscope to measure the modulation frequency and view the harmonic waveform of the lamp current.

This leaves just the third element of the system, photography. There are many types of cameras and film. The overriding consideration, however, is the amount of light that is reflected by the bubble to the camera. Although the bubbles seem bright to the eye, the light is somewhat marginal photographically. Thus we are forced to use extremely sensitive films, together with a camera which has a fast lens and as large a frame size as possible. In view of

this, almost all our photography to date has been still work. We have also tried some motion pictures and video tape with fair success. More work along these lines is essential to study truly unsteady flow patterns where a time history is required for proper interpretation of the flow phenomena.

What do the bubbles look like in a photograph? When the shutter is opened for a time T, a number of bubbles equal to RT come into the field of view of the camera. Each bubble leaves an image of its path, or a streak, on the film and this streak becomes a record of the air movement within this time frame. The record of a number of streaks on a single photograph produces a history of the air motion. The density of each streak on the film is not dependent on shutter speed, but rather on the aperture and bubble velocity V, as well as the sensitivity of the film itself.

If the camera views a field of dimension L, then the number of bubbles seen by the camera at any instant of time is given by RL/V. During the exposure, some of the bubbles will pass all the way through the field of view while others either start or end in the picture. The number which pass all the way through is given by (RT - RL/V). Going back to our earlier example, with R = 500 bps and V = 100 fps, and taking T = 0.1 sec and L = 5', we find that 25 bubbles will be imaged on the film at any instant. Also, over the duration of the exposure, 25 streaks will span the photograph. These relationships, of course, are oversimplified since they are based on a steady bubble generation rate, linear bubble paths and constant bubble velocity. Nonetheless, they do serve to indicate the role of the various parameters in streak photography.

An important point should be made here concerning the bubble production rate. To record a desired number of streaks, the shutter speed needed is inversely proportional to R. This is the principal motivation for wanting R large. Then T can be shorter, reducing in turn the exposure of any stationary object within the field of view of the camera, particularly the background. The result is a higher contrast streak photograph.

On the other hand, we do intentionally vary the number of streaks within a set of photographs of the same flow pattern. A relatively large number of streaks provides an overall picture of the flow pattern. We often go to a much smaller number, though, to see details of the air motion that are evident only by following individual streaks for an appreciable distance.

One final comment should be made on the system with regard to tunnel contamination. Since the wall thickness of each bubble is extremely thin, say on the order of 1/2 μ, very little bubble film solution is used. For example, we can manufacture, ideally, 65,000 bubbles 1/8" in diameter with each cc of solution. At a production rate of 500 bps, this amounts to 130 sec, or over 2 min of running time. In reality, not all the solution goes into good bubbles. A

small fraction emerges either as spray or heavy bubbles. Any solution that is deposited within the tunnel and on the model, we clean up very easily.

1.3 Representative Photographs

With the overall description of the flow visualization system in hand, we can examine the results - that is, the streak photographs themselves. The following examples are representative of the best pictures taken to date, yet by no means are they the best attainable. They clearly demonstrate the substantial advantages of the technique and provide a strong incentive to proceed further.

The visualization of the flow past a two-dimensional Kármán-Trefftz airfoil is reproduced in Fig. 3. The flow direction is from right to left. The pattern traced out by the bubbles is strikingly similar to classical smoke photographs, but with some important differences. Most evident is the turbulent separation

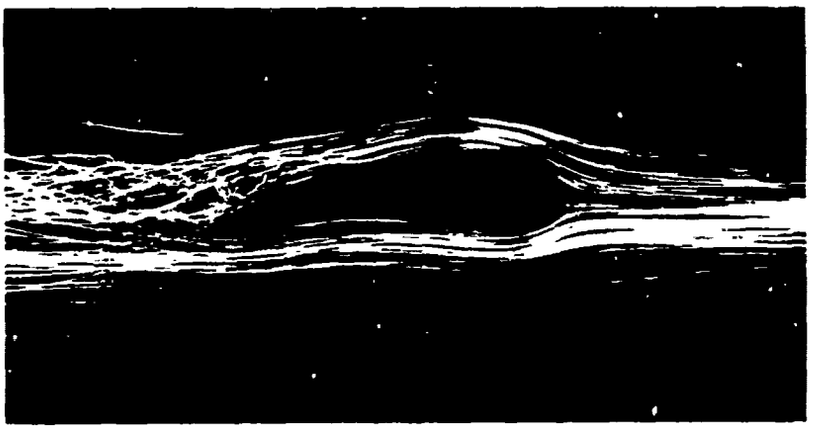

Figure 3. Flow About 2-D Kármán-Trefftz Airfoil

region above the rear portion of the airfoil. *For the first time we can see the air motion within it!* Smoke would diffuse and disappear here.

A more subtle difference is seen upstream, quite a bit ahead of the airfoil. Note how the bubble paths cross each other, though they have similar shapes. This is due to the low, but finite, level of turbulence characteristic of even the freestream tunnel flow. It can be somewhat disconcerting for people who expect to see only laminar flows. The photograph has recorded the fact that bubbles which pass through the same point upstream of the airfoil do not fall

exactly on the same trajectory thereafter. Essentially, the flow is just quasi-steady.

Some of the bubble streaks near the trailing edge divide into two parallel streaks. This happens because the light reflected by a bubble to the camera comes from two very small highlights that are aligned with the light beam. When a bubble moves parallel to the light beam, these two highlights follow the same path, producing a single streak on the film. If, on the other hand, a bubble has an appreciable velocity component normal to the light beam, the highlights then move along separate but parallel paths. The reinforcement of the image makes the single streak brighter than either of the separate streaks.

In this photograph, the bubbles are about 6" inside the tunnel window. Since the airfoil is flush with the window, the end appears larger than the section over which the bubbles are passing. This masks a small portion of the field right next to the surface so that we cannot see the leading edge and the details of the stagnation point.

With the lamp alone downstream, we would normally have a shadowed region upstream of the airfoil. To fill in this region, we used a projector mounted overhead. The areas in which the light beams overlap are evident by the pronounced increase in brightness, to the point where the streak images are overexposed and merge into each other. Between these two regions, we have only the projector light and the streaks are considerably fainter. From about the quarter-chord downstream, only the arc lamp illuminates the bubbles.

The next photograph, see Fig. 4, is a closeup view of the separation region above the same airfoil. The angle of attack of the airfoil has been increased

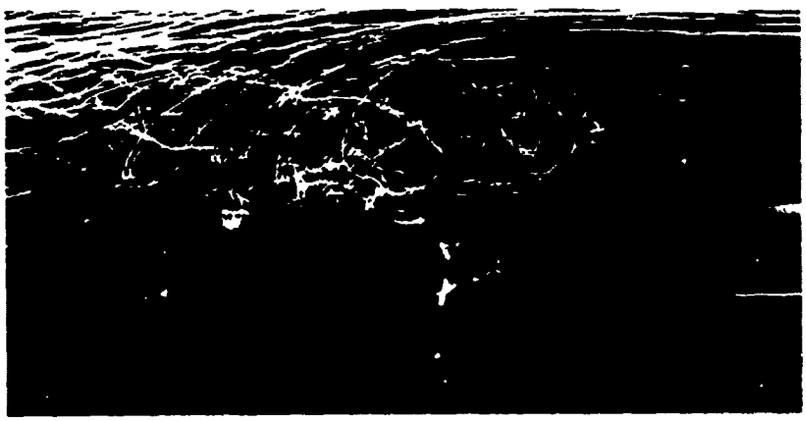

Figure 4. Closeup Of Separated Flow Region On 2-D Kármán-Trefftz Airfoil

here to enlarge the extent of the separation. A camera position slightly below and behind the trailing edge was chosen. The portion of the trailing edge within the light beam appears as a short, vertical bright line. Some droplets of bubble film solution on the lower surface show up directly upstream. As before, the upper surface of the airfoil is blocked by the near end of the model. It is actually located just below the curve defined by the upstream ends of the bubble streaks.

The main reason we selected this photograph is to illustrate how durable the bubbles are in a highly turbulent flow and how well they respond to rapid changes in direction. In fact, in some cases they seem to change direction almost instantaneously. Note again the twin streaks that we discussed in Fig. 3.

Finally, we call attention to the "straight" streak near the bottom of the photograph. This streak was created by one of many tiny styrofoam particles present in the flow. They arose from fairing pieces which broke away from inside the tunnel during a prior high speed run and persisted as a residual contamination. These appeared in several photographs and emphasize the importance of neutral buoyancy.

The last photograph is quite different. It is an overall view of the tip vortex trailing from a finite-span, constant-chord airfoil. The resulting flow

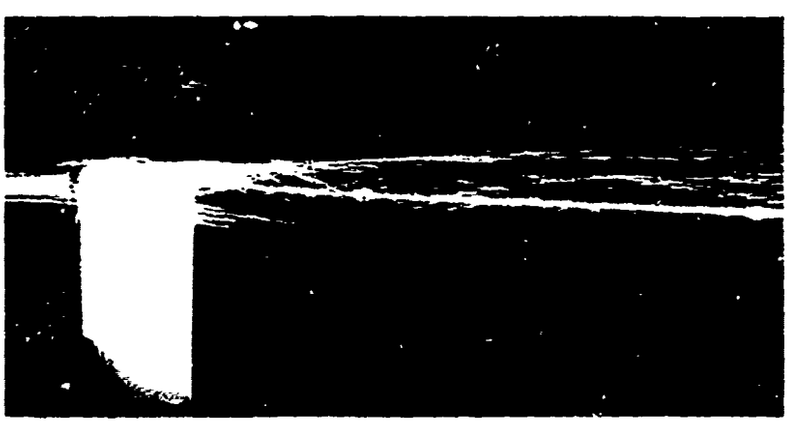

Figure 5. Tip Vortex From Finite-Span, Constant-Chord Airfoil

pattern is shown in Fig. 5, this time with the flow moving from left to right. The blade, or wing tip, is seen on the left with the suction surface toward the

camera. Upstream, the bubbles approach the tip along simple, rectilinear paths.

Downstream, however, the pattern is extremely complex, the wing tip imparting a pronounced rotation to the flow about a central axis or core. This core appears as a brilliant, solid tube since many bubbles spiral in near the tip and move downstream inside it. The rotational motion about this core is in the clockwise direction, facing downstream. It increases as we move outward radially from the center of the core, rises to a peak value and then decays. This rotation, combined with the axial motion and a small radial motion, produces helical bubble paths with changing pitch and radius. This creates the beautiful "basketweave" pattern that is captured in the photograph.

Although the tip vortex is often called wake turbulence, the orderliness of the flow is apparent. Still, the pattern is unsteady enough so that only the core is discernable with smoke visualization. To our knowledge, this photograph constitutes the best description of a tip vortex in air that exists.

2 WIND TUNNEL TESTS

2.1 Tests And Objectives

During the course of the investigation, three wind tunnel test programs were conducted. Each one served a somewhat different purpose. Collectively, they were designed to measure the performance of the system under realistic operating conditions. This played a key role in the development of the different system elements.

The first test program was carried out in the 3' x 3' Pilot Wind Tunnel at the National Aeronautical Establishment (NAE) in Ottawa, Canada over the period from 21 April to 6 May 1970. The objectives were twofold. First, since the test was preceded by a period of development of the head, lighting and photography, we wanted to establish the feasibility of the integrated system at that point and obtain the first good set of streak pictures. Second, we sought to define, at least qualitatively, the accuracy with which the bubbles can define a flow pattern. To meet these objectives, we selected a modest size tunnel that would allow us to photograph the bubbles from a fairly close distance. Also, we wanted to use a two-dimensional model so we could calculate the exact potential flowfield for comparison with the bubble traces. A Kármán-Trefftz airfoil was picked for this model.

The objective of the second test program was to utilize the system, together with any improvements, in a support role for an ongoing test. This led to our participation in an experimental investigation by Rochester Applied Science Associates (RASA) on the problem of tip vortex control. The test was run in the 8' x 10' Subsonic North Wind Tunnel at the Naval Ship Research and Development Center (NSRDC) at Carderock, Maryland. Our effort covered the period from 3-5 November 1970. It was our first opportunity to try the system in a large-scale wind tunnel facility.

The third and last test program was to apply the system as an actual investigative tool. Coincidentally, we had chosen the tip vortex as the flow pattern to study here prior to our work with RASA. We set up this test in the Subsonic South Wind Tunnel at NSRDC which is almost identical to the North Tunnel. The test was made in the period from 14-16 June 1971. For a model, we obtained a surplus rotor blade from a Navy HR2S-1 helicopter and cut off a section about 5 1/2' long from the tip. This rotor blade has a 24" chord. With such a large scale, we could see the details of the vortex formation more easily than in the RASA test where the chord was only 8".

2.2 Kármán-Trefftz Airfoil Test

The Kármán-Trefftz airfoil test program was our most extensive program. It involved 10 days of tunnel occupancy and approximately 32 hours of productive testing. In all, over 300 photographs were taken of the bubble motions.

The two-dimensional Kármán-Trefftz airfoil is essentially a more general version of the classical Joukowski airfoil. A computer program was written to plot the airfoil and the streamline pattern to enable us to generate a wide choice of different airfoils at several angles of attack. We finally settled upon an airfoil with a camber of 8% and a thickness ratio of 20%. It has a 9" chord and 10° trailing edge angle. The span of 36" is equal to the width of the Pilot Tunnel test section.

Before the test, the NAE installed special plexiglass windows on the ceiling and walls of the test section for viewing and lighting. The bubble generating head was positioned about 5" downstream of the test section entrance and 6" from the side wall containing the observation window. The head employed was our modified high-speed head which is somewhat larger than the prototype version[1]. The airfoil model was mounted midway between the floor and ceiling with its leading edge 45" downstream from the tip of the head. A view of this set-up from the diffuser of the tunnel, looking upstream, is given in Fig. 6.

Initially, we illuminated the bubbles with a 40° beam angle xenon arc lamp placed above the test section and the beam aimed vertically downward through the ceiling window. After a few tests, we changed to the 8° beam angle lamp and relocated it approximately 12' downstream from the airfoil in the tunnel diffuser, directing the beam upstream as described earlier. The downstream configuration was clearly superior and was adopted for all subsequent tests. As a forerunner to the optical shroud, we fabricated a simple cylindrical snoot for the lamp. This confined the beam and kept any light from striking the sides, floor or ceiling of the test section.

To improve the contrast between the illuminated bubbles and the background further, black flocking paper was applied to the back wall of the test section. Also, the observation window and camera were totally enclosed with an arrangement of black felt drapes. This eliminated any stray light. We set the camera from 14" to 40" away from the window, depending upon the field-of-view desired, but generally in line with the spanwise axis of the airfoil. In some cases, a 300-watt slide projector was utilized to fill in the shadowed portion of the flowfield caused by the airfoil in the primary light beam. The projector was situated overhead, immediately above the ceiling window. Its lens can be seen in Fig. 6 at the top of the picture. Black felt was also laid over the ceiling window to cut off any other light.

The maximum test section velocity possible was 150 fps with the original fan

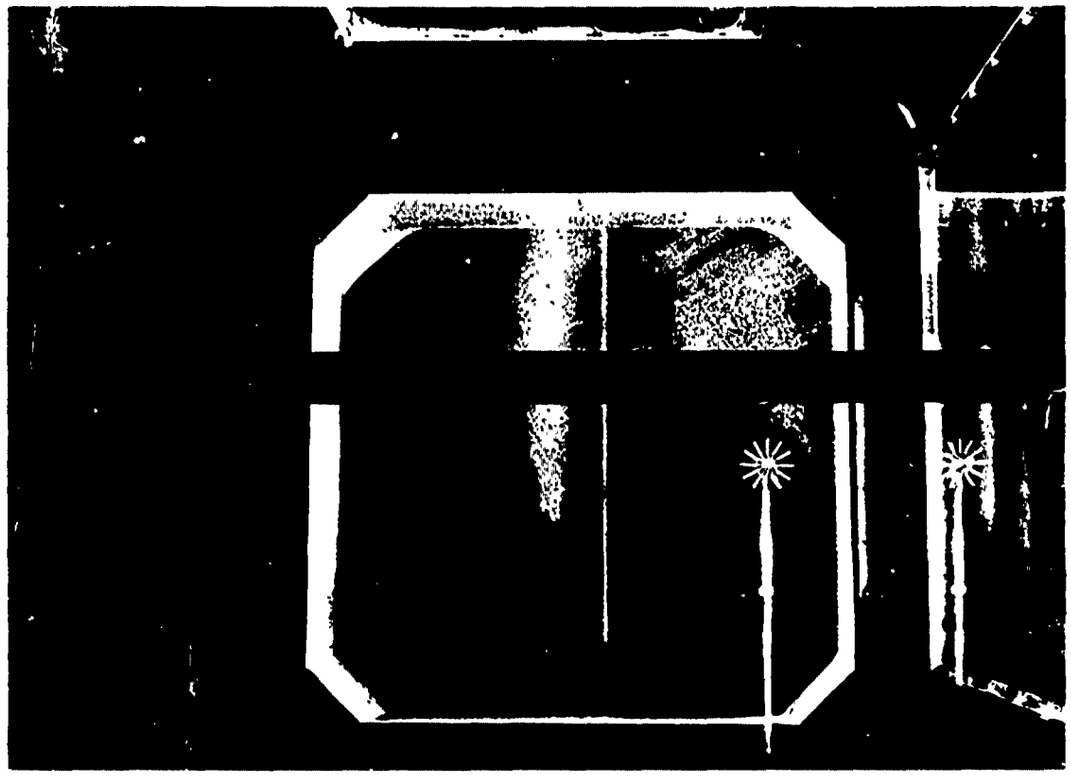

Figure 6. Wind Tunnel Setup For Kármán-Trefftz Airfoil Test

blade settings. We conducted our shakedown tests with these settings. Afterward, the NAE reset the blades to try to reach 200 fps top speed. Recalibration of the tunnel indicated that we could just reach this speed at about the limit on the current to the fan motor. Under these conditions, unfortunately, the airstream heated up quite rapidly, reaching temperatures of 135°F and higher in 5 min or less. At the higher velocities, therefore, we adjusted the head and camera with the tunnel at a lower speed, typically 100 fps. Then the tunnel speed was raised quickly and photographs taken of the bubble streaks before the air temperature became excessive. Otherwise, our procedure was to set and focus the camera, raise the tunnel speed to the desired value, check the constituent flowrates to the head for optimum bubble size, density and production rate, and finally take the photographs.

We obtained photographs at 14 combinations of tunnel velocity and airfoil angle of attack. The tunnel velocities were 50, 75, 100, 150, 175 and 200 fps and the angles of attack were -5°, 0°, 5° and 10°. Except at -5°, separation over the upper surface was evident. This separation was exaggerated locally by the wake from the head. In fact, the spanwise variation in lift across this region produced a system of trailing vortices. These vortices show up nicely in the photographs. Though unexpected, the wake effect of the head did not compromise our test objectives. It only meant that we had to go to lower angles of attack and higher speeds for our accuracy comparison. Finally, -5° and 100 fps were used.

Much of our time was devoted to finding the proper camera exposures for the different tunnel velocities. With the 8° lamp downstream and the projector overhead for fill-in, the f-stop was varied from $f/5.6$ down to $f/2.8$. The shutter speed was varied, too, to establish which settings gave enough traces and defined the flowfield fully without obscuring the details. This ranged from 1/10 sec to 1/2 sec.

A large number of the photographs are excellent with intense bubble streaks. Since low f-numbers were required, the depth-of-field is limited and the streaks removed from the center of the light beam are somewhat out of focus. The only real difficulty encountered was the air temperature rise when testing at the top speed of 200 fps. From our observations, the bubbles performed well initially when the temperature was below 100°F, say. But, with further heating, the bubbles broke up in passing over the model.

In addition to the still streak photographs, we tried a high-speed motion picture with a Milliken framing camera furnished by the NAE. Tri-X negative film was used at a framing rate of 500/sec. The results were rather marginal, basically due to the lower film sensitivity compared to the still film. The question of film sensitivity will be discussed later.

2.3 RASA Support Test

The principal objective of RASA was to determine the effectiveness of a jet of air, directed rearward from the tip of a finite wing or rotor blade, as a means to dissipate the strong rotational motion of the trailing vortex. Our visualization served mainly to locate the vortex core for other probe measurements and to show qualitatively the results from blowing. At the same time, we made our first attempt to obtain quantitative data with the modulator which was designed and built after the previous test.

Setup of the system was rapid and relatively easy. The elapsed time required was about 2 hr, at least half of which was spent outside the tunnel so that it did not interfere with the testing in progress. The high-speed head was clamped to a rod as described earlier for Fig. 2. This rod was mounted vertically in the tunnel contraction section, 9' upstream of the model. The model was a semi-span wing with a constant 8" chord. It extended 30" vertically from the floor of the test section. Further details on the model and its blowing characteristics are given in Ref. 12. The optical shroud with the high-intensity lamp was attached to a stand 16' downstream of the model. A photograph of this setup from upstream is presented in Fig. 7. The equipment seen between the model and the lamp is not part of the visualization system, but a traversing mechanism for the probe measurements.

The test conditions that we photographed included airfoil angles of attack of 7° and 10°, tunnel velocities of 50 and 100 fps, and blowing rates from 0 to 0.8 cfs. To begin with, we took 2 rolls of film, or a set of 24 photographs, with different camera settings to establish the desired apertures and shutter speeds. These test rolls were developed overnight and examined before any more photographs were taken. Then we took six production rolls, for a total of 96 photographs.

Three different camera angles were tried, one from above looking along the span of the model and two from the side. From above, the shots were made only upstream with the model included in the pictures. From the side, we photographed both upstream and downstream. The upstream shots covered the flow from about 1 chord ahead of the model to 6 chords behind and the downstream shots from 6 chords behind to 13 chords behind.

For 30 of the photographs we modulated the light source at frequencies from 125 to 1000 Hz, concentrating on 250 Hz. From these, we were able to calculate the axial velocity component at various distances from the vortex core, both inboard and outboard of the airfoil tip. We could also calculate the rotational and radial velocities. The details of these calculations, along with an example of the modulated pictures, will be incorporated in *Section 3.2* with our discussion of illumination and modulation.

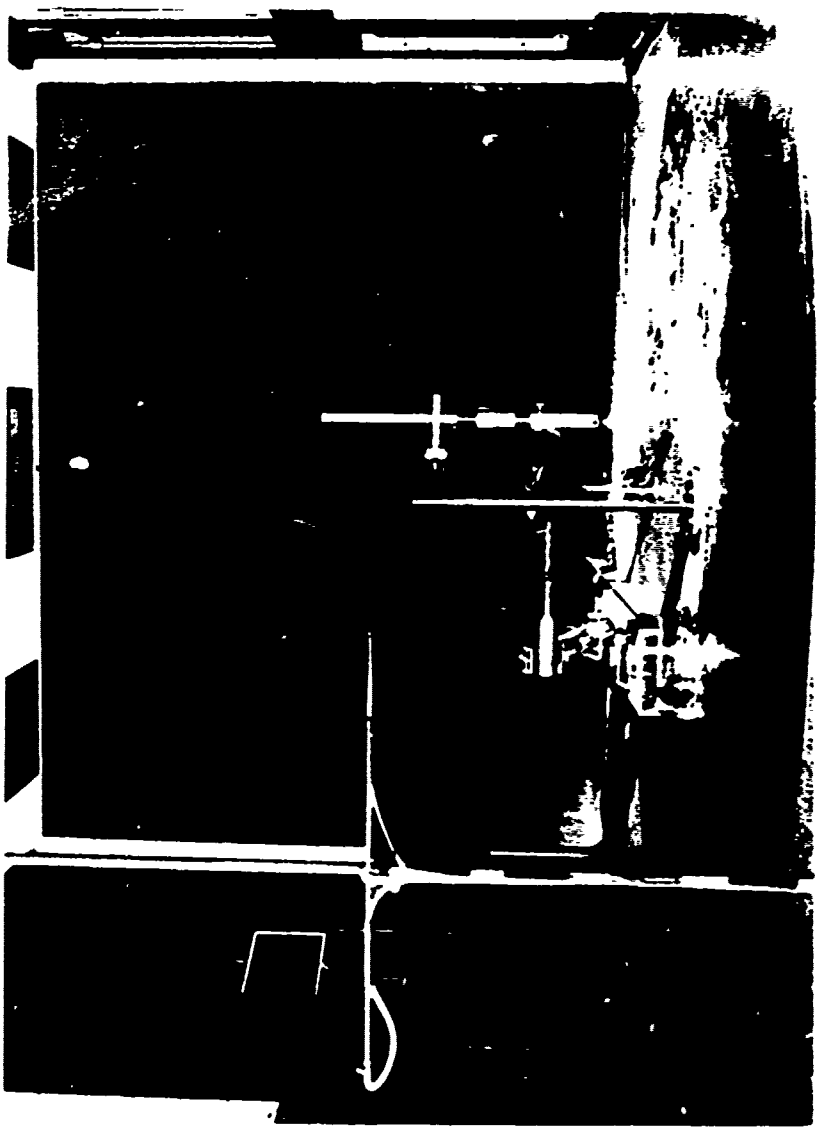

Figure 7. Wind Tunnel Setup For RASA Support Test

This test, above everything else, demonstrated the simplicity and adaptability of the technique. The most dramatic part was to see the tip vortex so vividly portrayed, as illustrated in Fig. 5. Beyond that, the test qualified modulation as an important new dimension to the system, providing a unique capability to measure instantaneous velocities within complex flowfields.

2.4 HR2S-1 Blade Tip Vortex Test

This test program was directed basically at visualization of the formative stages of the tip vortex. The tip vortex is a complicated, three-dimensional flow pattern which remains poorly understood despite all the work that has been done on wing and rotor aerodynamics. Our main emphasis was on getting good streak photographs, both from an end view and a plan view. We also took this opportunity to try movie and stereo photography for the first time in a full-scale facility.

The 5 1/2' section cut from the HR2S-1 rotor blade was welded to a circular plate 2' in diameter. This plate was drilled with a series of holes at the periphery for different angles of attack. The whole model was painted with several coats of glossy black paint to improve the background for the bubble traces.

The base plate was bolted to the floor of the tunnel test section, the blade extending vertically to within 2 1/2' of the 8' ceiling. Prior to the test, we prepared a scale drawing of the tunnel to help us position the model for the best camera angles. The best position was a little upstream of the balance location, right under a small overhead window. This allowed us to photograph from above, or endwise, as well as from the side windows of the tunnel.

For most of the streak photographs, the bubble generating head was 6 1/2' upstream of the blade leading edge. The lamp and optical shroud were fastened on a stand in the tunnel diffuser 13' downstream of the blade trailing edge. A photograph of this setup taken from downstream near the lamp, looking upstream, is shown in Fig. 8.

We took 18 rolls or 216 streak photographs in all, 66 of which were with lamp modulation. To optimize the photography, we ran at a tunnel velocity of 50 fps and an angle of attack of 8°. We tried some photographs of the vortex wake, 2-3 chord lengths downstream of the blade trailing edge, with 4 rolls of film. For these photographs, we moved the lamp 10 1/2' further downstream. Exposures, in general, were based on the results from 3 test rolls taken the first day and developed overnight.

The purpose of taking movies was to explore their potential for enhancing the information we get. Movies, or at least sequence photographs, may be essential

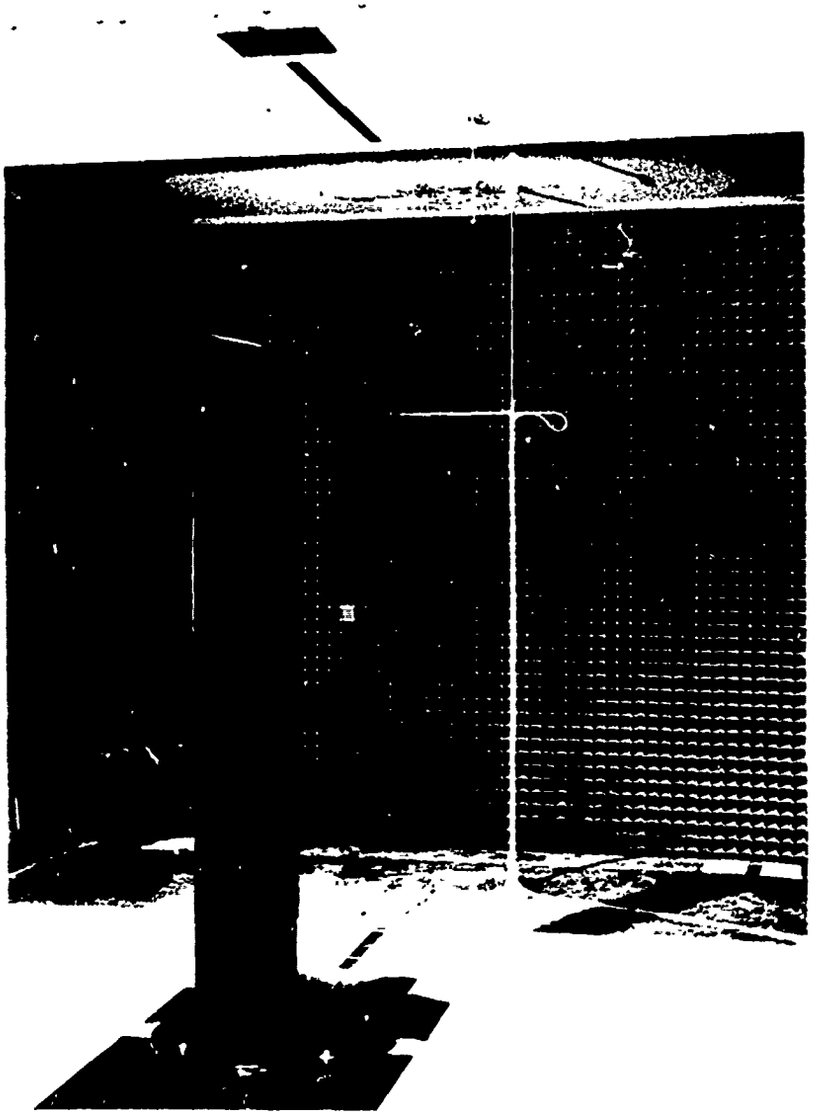

Figure 8. Wind Tunnel Setup For HR2S-1
Blade Tip Vortex Test

if the flow pattern is unsteady. We shot 4 rolls of 16 mm film, totalling 500' in length. This was broken down into 32 sequences, each 15' to 16' long. The normal filming speed of 24 frames per second was employed throughout.

For some of the movies, we moved the model downstream onto a turntable at the balance location. We were then able to vary the angle of attack of the blade continuously to produce a time-varying vortex pattern. Starting at 0°, we increased the angle of attack 6° past the nominal stall angle of 14° to 20° and back down again. This allowed us to see the buildup of the tip vortex, followed by a complete breakdown of it as the blade went into deep stall.

We had hoped that stereo photography would provide a good way to study three-dimensional flow patterns. Unfortunately, our experiment here was unsuccessful because the camera employed had too slow a lens and too small a negative size. We took 60 exposures in all, but the streaks were too weak to show up distinctly. Still, we feel that stereo photography will ultimately prove very useful.

In summary, we got some excellent photographs from this test which afford a unique insight into the formation of the tip vortex. We were also able to examine the potential capabilities of movie and stereo photography, both of which should be pursued. The visualization system performed extremely well. It was easy to set up and completely reliable.

3 SYSTEM ELEMENTS AND DEVELOPMENT

3.1 Bubble Generation

The three elements which were developed for bubble generation are the head, console and bubble film solution. We described the console earlier and, since most of its development took place prior to the present work, we will not discuss it further. If needed, details can be obtained from Ref. 13. A good deal of head and bubble film solution (BFS) development, on the other hand, was accomplished between the work reported in Ref. 1 and the test at the NAE on the Kár‚ án-Trefftz airfoil.

The design and testing of the prototype high-speed head was originally discussed in Ref. 1. For reasons of simplicity and compactness, we first sought to accelerate the bubbles up to the freestream velocity in the mixing region downstream of the head. The layout of this design is reproduced in Fig. 9.

Basically, the upstream portion of the head is an enlarged version of our low-speed head[1] with the same tube arrangements and sizes. The downstream portion is a removable shroud which protects the bubble as it is formed. Between the two is a small plenum for compressed air brought in through the support rod. After the air passes through the porous plug to smooth the flow, it serves to separate the bubble from the tip of the 16 gauge tube. The bubble is then carried out into the freestream within this jet of air. Helium enters the head through the 11 gauge tube farthest upstream of the stem and BFS through the intermediate tube.

We evaluated the performance of the prototype high-speed head principally on the basis of the maximum freestream velocity into which bubbles could be successfully implanted. The head was tested with 5 different shrouds. The best performance was achieved with a boattail shroud that had a ℓ/d ratio of 6. Here ℓ is the distance from the tip of the 16 gauge tube to the shroud exit, and d is the inner shroud diameter. With this shroud, the head operated well at freestream velocities up to about 125 fps.

The principal mechanism responsible for breaking up the bubbles at the limiting implant speeds was the turbulent mixing immediately downstream of the head. The effect of changing shrouds was to modify the severity of this mixing. In Ref. 1, we suggested various improvements that we felt would help to raise the limiting implant speed. Most of our subsequent effort followed along these lines.

The improvements fall into three areas. First, and most obvious, we tried to suppress the turbulent mixing. Second, we attempted to tailor the air flow

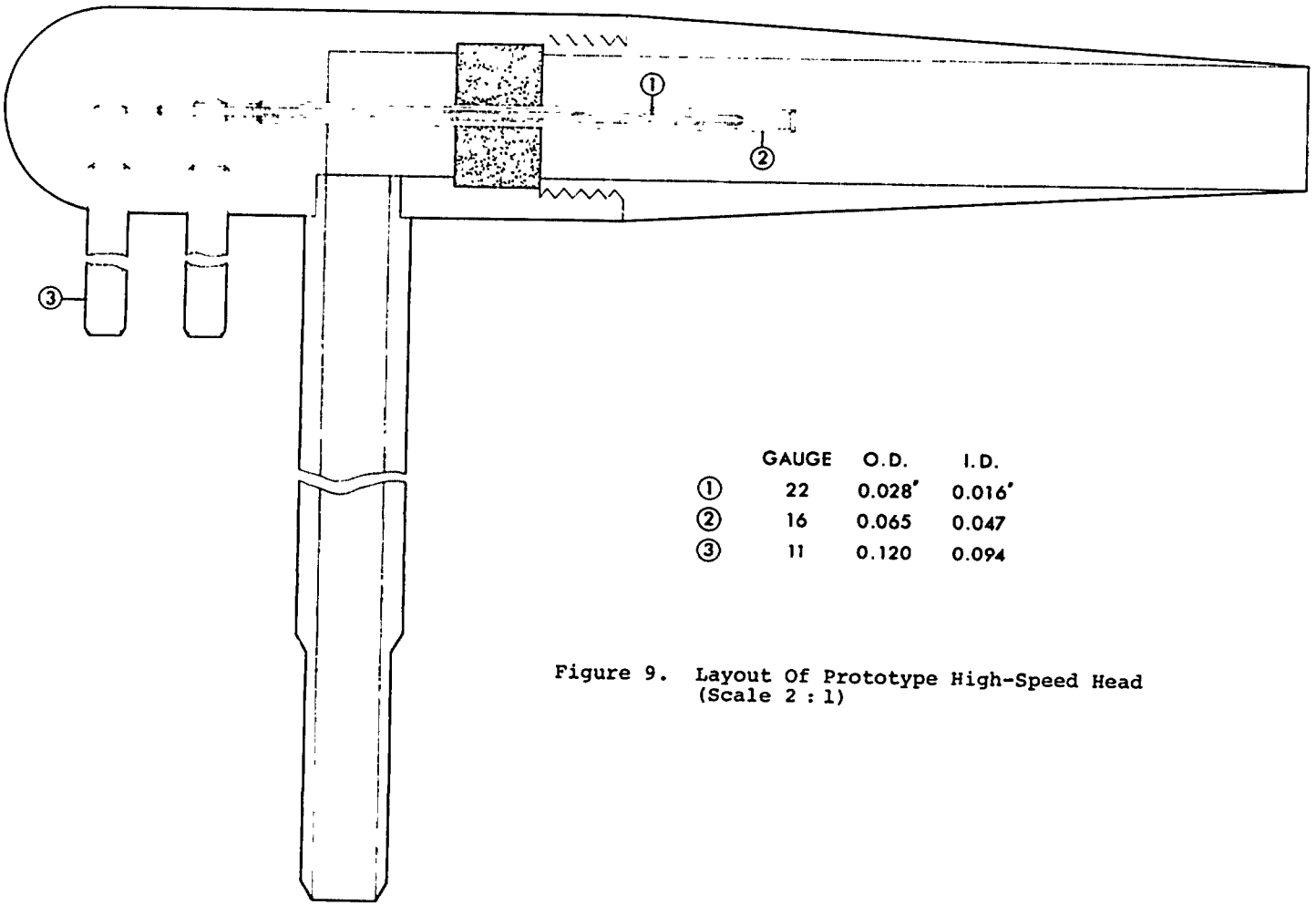

	GAUGE	O.D.	I.D.
①	22	0.028"	0.016"
②	16	0.065	0.047
③	11	0.120	0.094

Figure 9. Layout Of Prototype High-Speed Head (Scale 2 : 1)

inside the shroud so that the bubbles would come out along the shroud axis. This would eliminate the problem of bubbles hitting the inside of the shroud and introduce them into the mixing region along the axis away from the most severe turbulence at the periphery. Third, we experimented with new bubble film solutions that would produce more elastic bubbles capable of withstanding greater deformation in turbulent regions.

One direction we took on the mixing problem was to study some recent work on coaxial jets. Our problem is somewhat unique in that the jet issues from the head at a lower velocity than the freestream, typically 15-30 fps versus 100-200 fps, say. This same situation is encountered in the coaxial configuration of a gas-core nuclear rocket in which nuclear fuel is contained within a low-velocity central jet surrounded by one or more faster-moving annular jets of propellent. Mixing between the two leads to loss of fuel and a fuel density too low for criticality.

Although we did not find any direct application to our problem in terms of modifications to our head design, the results of Refs. 14 and 15 were quite helpful. These results pertain to the photographic investigation of a bromine jet issuing coaxially into an outer stream at stream-to-jet velocity ratios of 0.4 to 32. The downstream mixing is observed to be laminar, provided that the jet Reynolds number and this number times the velocity ratio are less than 2400 and 3400, respectively. The first criterion appears to mean simply that the inner jet must be laminar since a Reynolds number of 2400 is appropriate to the transition between laminar and turbulent flow in smooth pipes. If we extend these bromine/air results to our air/air case, they imply that the outer airstream must be typically less than 30 fps to have laminar mixing. Therefore, the elimination of turbulent mixing entirely seems rather remote.

With this direction blocked, we turned to the alternate scheme offered in Ref. 1, i.e., to accelerate the bubbles within the head, rather than downstream, so that the jet emerges at the freestream velocity. Then the bubbles would only be exposed to the mixing from the boundary layers on the inner and outer surfaces of the shroud. This approach necessarily leads to a larger head in order to allow for a contraction within the shroud.

Accordingly, a new, modified high-speed head was designed and constructed. The overall diameter was scaled up from 5/8" to 1 3/8". The shroud, instead of a constant inner diameter of 3/8", was tapered from a diameter of 27/32" around the tip of the BFS tube to 3/8" at the exit. The total included angle of the taper is 8°. This first shroud was made to give jet exit velocities of about 200-250 fps, but we provided the flexibility so that additional shrouds could be substituted for different exit velocities.

Simultaneously, we worked on improving the internal air flow characteristics

of the prototype head. We began by replacing the porous plug with a honeycomb array of tubes. This was composed of 30 individual 16 gauge tubes, 1/4" long, cemented together in a tightly packed parallel arrangement. Testing the head in still air with the honeycomb, we found that the performance was markedly better, not only in terms of the measured velocity profile at the exit but also in terms of the initial behavior of the bubbles. Very few bubbles hit the inside of the shroud and the dispersion was greatly reduced.

Based on this improvement, we fabricated a similar, larger honeycomb for the modified high-speed head from 36 individual 11 gauge tubes, 1/2" long. The performance of this head was then tested, again in still air. The bubbles accelerated nicely and the desired bubble size, density and generation rates were achieved with about the constituent flow rates predicted.

In addition, we experimented with the introduction of a swirl component into the axial flow within the shroud. We hoped that this rotation would stabilize the bubbles even more and cause them to move along the axis of rotation on out into and through the mixing region with the outer flow. Another possible bonus might come from the unusual axial velocity profile that some swirl flows exhibit. This profile has a minimum at the axis and peaks near the wall, blending well with the high-speed outer flow.

To introduce the swirl, we built up two swirl plugs and a swirl section for the modified high-speed head. The plugs replaced the honeycomb flow straightener and generated a fixed amount of swirl. One plug had four sets of five holes aligned tangentially to the inner radius and the other, a single slot. The swirl section, on the other hand, was a cylindrical piece fitted between the upstream portion of the head and the shroud. It was approximately 1" long and had four inlets distributed around the periphery to inject secondary air tangentially to the inner surface. By controlling the amount of secondary air, different degrees of swirl could be imparted to the primary air flow which entered as before through the honeycomb flow straightener. Both of the plugs and swirl section gave rise to a certain amount of turbulence in the internal flow. This is extremely difficult to avoid in creating any swirled pipe flow unless long sections are employed. We thought, though, that whatever positive effect of swirl we got would outweigh any negative effects of turbulence.

Prior to testing these elements, we built several other elements. The modified head was initially designed with larger helium and BFS tubes than in the smaller prototype head to allow for higher air velocities within the shroud. This was not realized and the bubbles were too big, i.e. 1/8" to 3/16" in diameter. To produce smaller bubbles that we felt would be more durable, we made a second upstream section for the modified head with the same tube sizes as shown in Fig. 9. Also, we made a finer honeycomb from 172 lengths of 16 gauge hypodermic tubing, as well as a constant diameter shroud for this head

with an ℓ/d of 6. With these elemcnts in hand, we carried out a systematic program to test the performance of different combinations of the two modified hi -speed heads, the two swirl plugs, the swirl section, the new honeycomb straightener and the two shrouds.

The tests were conducted in the SAI 6"x 6" Wind Tunnel which was constructed specifically for these tests. With this facility, we were able to perform more extensive tests more efficiently than if we had to go to an outside facility at this stage of development. The tunnel is an open circuit, suction design driven by a centrifugal blower. The test section is square, 6" on a side, with removable side panels. It has a length of 3' so that the bubble acceleration process can be studied downstream of the head. The area ratio of the contraction section is 9:1 and the included angle of the diffuser is 5.4°. A constant-area section between the diffuser and blower is equipped with slots, to accept various porous plates, and doors to let in bypass air. These allow us to adjust the test section velocity continuously from 25 to 250 fps. Uniformity in velocity over any cross section is better than ±2%.

Turning now to the test results, we found a very positive effect of going to smaller bubbles, about 1/16" to 1/8" in diameter, and the finer honeycomb. The dispersion of bubbles within the shroud was cut down to the point that virtually all of the bubbles passed out of the shroud without touching the inner surface. Still, they exited from the shroud at apparently random and continually changing locations. Farther downstream, the dispersion was also less, but still appreciable. The contracting shroud performed better in this regard than the constant diameter shroud.

With the swirl plugs, many of the bubbles were excellent but many, also, were centrifuged out to the shroud wall and left as spray. It appeared that the swirl was so strong that only the lightest bubbles remained within the jet. With the contracting shroud we observed a rapid decrease in axial velocity near the centerline, as we expected, but with the constant diameter shroud we actually saw reverse flow at the centerline with air entering the head.

To experiment with less swirl, we used the combination of the modified high-speed head with the finer tubes and honeycomb, the swirl section and the contracting shroud. With this configuration, we were able to implant bubbles successfully at the maximum velocity of our tunnel which is just over 200 fps with the blockage from the head. This was achieved with virtually no bubbles bursting either within the shroud or downstream and with minimal dispersion. The secondary air had little effect on the results, though, regardless of the amount used. A modest amount of air did slightly reduce the dispersion of bubbles downstream, but the bubbles did not exit from the shroud along the centerline as we had hoped.

With further testing, we discovered that the improvement in performance actually came from tailoring the flow outside the shroud rather than the flow inside the shroud. This was attributed to the external air inlets on the swirl section. Therefore, we abandoned swirl altogether and devised a "sunburst" section which was installed in place of the swirl section between the upstream portion of the head and the shroud. The design for this section had twelve spokes, each 1/8" in diameter and 1" long, extending radially outward. These spokes reach gently into the freestream and induce a smooth, gradual shear between the freestream and the jet from the head. The new configuration performed very well and was selected for the Kármán-Trefftz Airfoil Test at the NAE. This is the head seen in Fig. 6. A detailed drawing is also given in Fig. 10.

Before this test program, we experimented with new bubble film solutions as well. Earlier we had used a mixture of a commercial bubble solution and glycerin[1]. However, from Refs. 4, 5 and 6, we felt that a significant improvement might be realized by trying different industrial surfactants. We worked principally with various Aerosol surfactants from the American Cyanamid Company and formulated an extensive number of mixtures with water, glycerin and, sometimes, sucrose or dextrose. These were tested first with a simple blowtube and then with our low-speed head. In turn, the most promising solutions were tested with the modified high-speed head in the SAI 6" x 6" Wind Tunnel.

We finally selected a mixture consisting of 50 ml of glycerin per 100 ml of a 15% Aerosol solution. With this high Aerosol concentration, the bubble generation rate was increased substantially over what we had obtained previously. The bubble film was thinner, too, and remarkably durable. Furthermore, we found the new solution, called 1035 BFS, is not toxic, corrosive or likely to stain anything.

The Aerosols are hydrocarbon surfactants. We also tested some fluorocarbon surfactants from the 3M Company. Although these surfactants are capable of lowering the surface tension more than the hydrocarbon surfactants, none of the solutions we formulated were nearly as good. The key to the high bubble generation rate appears to be the mobility of the surfactant molecules in reaching the new surfaces that are created very rapidly when the bubbles are formed. This mobility cannot be measured readily. As a consequence, a trial-and-error procedure is necessary to formulate effective solutions.

The 1035 BFS and the final configuration of the modified high-speed head were employed in the Kármán-Trefftz Airfoil Test. They performed very well in this test except for the heating problem described earlier and the apparent effect of the wake from the head on the separation above the airfoil. To avoid the wake problem, we went back to the smaller prototype high-speed head to see what

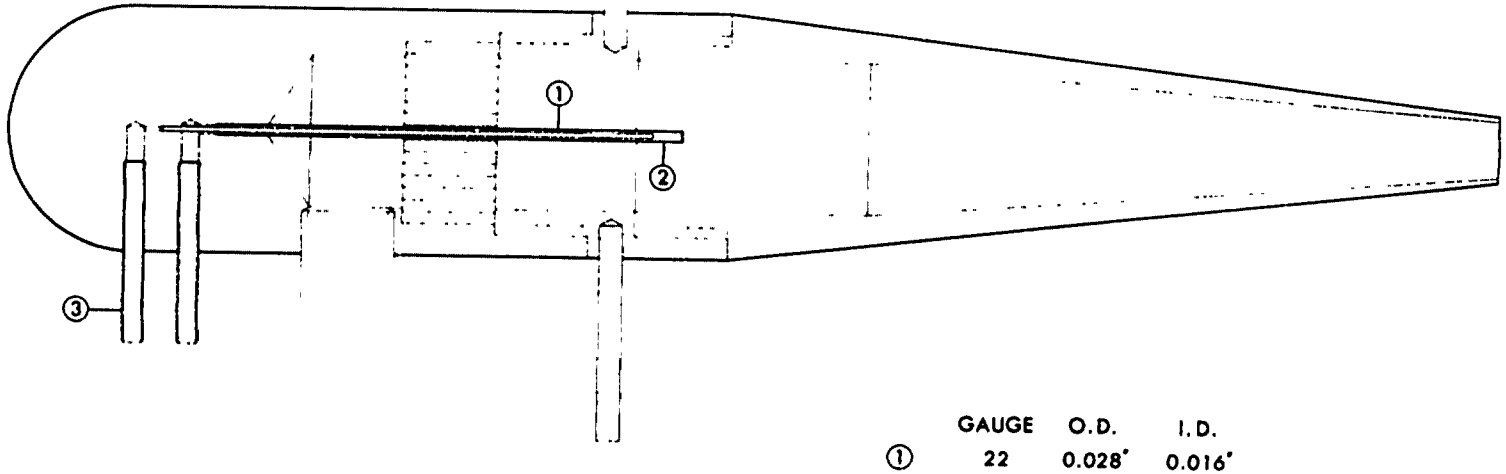

	GAUGE	O.D.	I.D.
①	22	0.028"	0.016"
②	16	0.065	0.047
③	11	0.120	0.094

Figure 10. Layout Of Modified High-Speed Head (Scale 1 : 1)

we could do. We first tried this head with the 1035 BFS in the SAI 6" x 6" Wind Tunnel. Surprisingly, the bubbles survived the acceleration up to the maximum speed of about 200 fps. We concluded that this result can only be attributed to the much greater durability of the bubbles.

In addition, we tried a scaled-down sunburst section on the prototype head. Though it did not seem to be required at speeds up to 200 fps, we thought this might allow us to go to higher speeds. Later on we also fabricated and tested two longer shrouds for this head with ℓ/d values of 8 and 10. As best as we could tell, there was no improvement over the shroud with an ℓ/d of 6 up to 200 fps. Nevertheless, we expect they may work better at higher speeds.

In the end, the final head configuration that we adopted for the second and third wind tunnel test programs was basically the original prototype head. The only differences from Fig. 9 are the substitution of the honeycomb flow straightener for the porous plug and the ℓ/d = 6 shroud for the ℓ/d = 4 shroud. This return to a more compact head clearly represented an exciting development for the present speed range. Still, the larger, modified head and associated technology may provide the essential means to achieve even higher speeds.

3.2 Continuous Illumination And Modulation

The development of an illumination scheme followed quite closely the recommendations set forth in Ref. 1. This entailed finding a small lamp giving an intense, well-collimated light beam which could be modulated in some fashion. The optical shroud was constructed for better light uniformity. To assist in the study of bubble formation, we also used a high-intensity strobe.

After looking at a wide range of light sources, we focused our attention on the Xenon Illuminator manufactured by the Eimac Division of Varian. This is a sealed-beam unit filled with high-pressure xenon gas. It has a short electrical arc as a source of light, with the electrodes aligned parallel to the beam axis in order to avoid shadowing problems. A reflector is integrated within the lamp and the window is made of sapphire for strength and good spectral transmission. The light output approximates that of the sun in the ultraviolet, visible and infrared ranges. Overall, the unit is rugged, shock-resistant and stable, with a relatively long life of about 1000 hours. It can be operated in any position with minimal cooling.

Of particular importance for our application was the size of the lamp and the narrow beam angle. The unit is extremely compact with a diameter of about 2" and a length of slightly over 2". It has a beam angle of 8° between the 10% points in the beam intensity distribution curve. The lamp has been modulated successfully to a depth of 90%. Pulsing, that is actually turning the lamp off and on, is possible, too, but it causes rapid deterioration of the electrodes.

Alternatively, a version of the lamp is available that images the arc in front of the window. This would be convenient if a mechanical wheel were used to chop the light instead of electronic modulation.

The Eimac lamp is available in two sizes, 150 watt and 500 watt. The 150-watt unit produces a peak luminous intensity of 250,000 candles, while the 500-watt unit puts out 1,000,000 candles. Altogether, though, the 500-watt unit costs over three times as much, including the power supply and holder.

We first conducted visual tests with a 150-watt demonstration unit in the SAI 6" x 6" Wind Tunnel, lighting the bubbles from upstream ahead of the contraction. The lamp was extremely intense to the eye and the bubbles appeared very bright at speeds on the order of 50 fps. However, the intensity of the bubble traces decreased rapidly with distance of the lamp from the bubbles and with increasing bubble velocity. We concluded, therefore, that this lamp was probably suitable for testing in wind tunnels of small to moderate size at modest velocities, but might be inadequate in larger tunnels and at higher speeds.

Besides the Eimac lamps, we briefly explored a much larger high-intensity lamp, the Lightsun Model XE-20 Sunlight Simulator built by Xenotech, Inc. This unit is a commercial version of a military helicopter searchlight with an upgraded power of 2000 watts. The beam divergence angle is good, 6.5° to 10°, and the unit can be modulated. It has a cylindrical light source, 11" in diameter and 18" long. Although the total cost is about nine times the Eimac 150-watt lamp, a unit this large might be essential for visualization in a large tunnel at high speeds. On the other hand, there is the problem of shadowing of parts of the flowfield by the model, so that several smaller lamps could prove mor suitable than one large one.

In view of all of these considerations, we decided that the 150-watt Eimac lamp would be adequate, at least for the first test program in the NAE 3' x 3' Pilot Wind Tunnel. To provide flexibility, we ordered a wide-angle 40° lamp as well as the 8° lamp. With the two lamps we were able to try lighting the bubbles both from within the diffuser and from above the test section, as described earlier. Unfortunately, the lamps cannot be run in parallel but they use the same holder and power supply.

The test program at the NAE confirmed the superior illumination obtained with the lamp in the diffuser. Still, the photographs showed a considerable variation in streak brightness. This we attributed to the nonuniform beam intensity distribution. It falls off in a Gaussian fashion with radial distance from the beam axis.

To achieve a more even light distribution for the following test programs, we designed and constructed the optical shroud. This shroud consists of two

condensing lenses, an iris diaphragm and a projection lens mounted in front of the lamp. The condensing lenses have a combined focal length of 200 mm and the projection lens has a focal length of 285 mm. A scale drawing is given in Fig. 11.

The optical shroud gives a uniform beam 16" in diameter at a distance of 12' from the lamp. What's more, with the iris we can reduce the spot size if desired without a loss in intensity or the iris can be replaced by a cutout of another shape for a non-circular beam. A 15' extension line that we installed between the lamp and power supply allows the power supply to remain outside the wind tunnel diffuser.

After the first test program at the NAE, we also developed the capability of modulating the lamp. But before we proceed, we should distinguish clearly between modulation of a continuous light source and a conventional strobe. A strobe lamp flashes on briefly for just a few microseconds during each cycle. As a result, the motion is frozen so that in place of a streak we see a series of bubbles. Only by connecting sequential positions of a single bubble can the bubble path and the velocity be established. If more than one bubble passes through the flowfield in a photograph, and the flowfield itself is complex and/or unsteady, it is impossible to tell which images are due to which bubbles.

In contrast, the lamp is on most of the time with modulation. The intensity is decreased for merely a small fraction of each cycle. This produces an interrupted or dashed trace instead and makes the individual bubble paths quite evident. Consequently, velocity measurements can be made directly from these traces.

The modulator was designed specifically for the Eimac lamp power supply. It is based on the principle of shunting a portion of the power supply current away from the lamp in order to reduce the light intensity. In operation, the lamp current is switched between the maximum value set by the power supply and a lower value set by a modulation depth control on the unit. Two other controls afford independent adjustment of the on-time and the off-time, that is the time periods of the maximum and minimum currents during each cycle.

The on-time can be varied from 50 to 8,000 μsec and the off-time from 50 to 5,000 μsec. To get the modulation frequency, we take the reciprocal of the sum of the two times selected. As an example, suppose we fix the frequency at 250 Hz with the lamp off during 25% of each cycle. This corresponds then to an on-time of 3,000 μsec, or 3 msec, and an off-time of 1,000 μsec, or 1 msec. Carrying the numbers a step further, we will see a dashed streak with each dash 0.3' or 3.6" long for a bubble moving at 100 fps. The dashes will be separated by gaps 0.1' or 1.2".

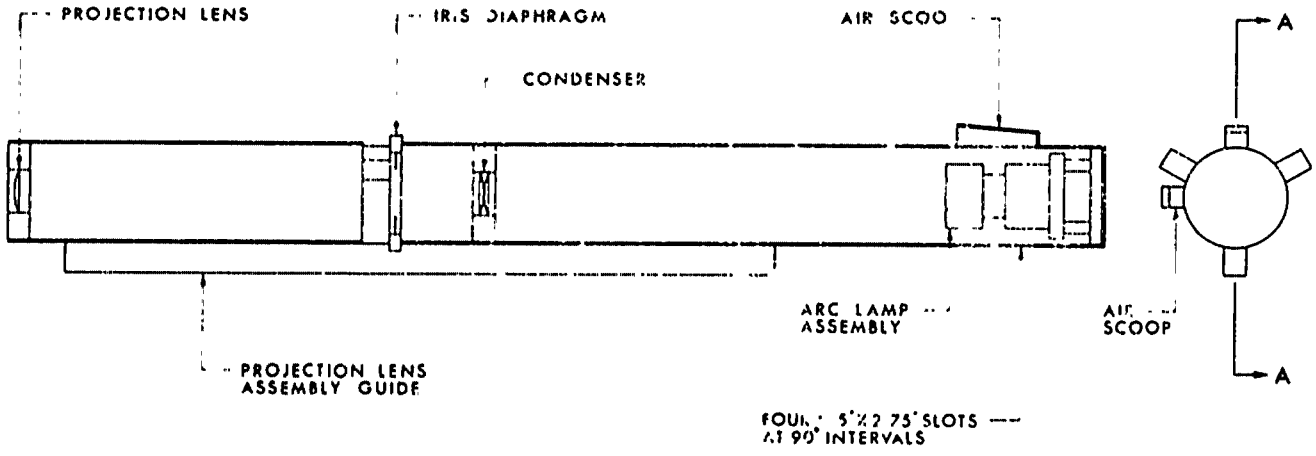

Figure 11. Drawing Of Optical Shroud Combined With Arc Lamp (Scale 5 : 32)

The modulation depth is the ratio of the difference between the maximum and minimum lamp currents to the maximum current. If the lamp is kept at the minimum level too long, though, the lamp will extinguish. As we shorten the off-time, we find we can run at greater depths of modulation. With our design, we can vary the modulation depth from 0 to 0.90. We have not measured the actual reduction in light intensity, but it seems to follow the lamp current very closely.

The modulator circuit is detailed in Fig. 12 and Table 1. Principally, it consists of a pulse generator and shaper, a controllable shunt switch, a protective circuit and a regulated d-c power supply. The protective circuit eliminates the high voltage transient that would otherwise occur when the lamp is accidentally extinguished due to excessive modulation. In addition, a terminal is provided to monitor the lamp current by means of the voltage drop across the lead wire between the lamp cathode and ground.

The optical shroud and the modulator were initially tested in the SAI 6"x 6" Wind Tunnel. For this purpose we modified the diffuser of the tunnel to illuminate the test section from downstream. Since the optical shroud is too big to be put inside, we introduced the light through a hole in the side of the diffuser. The light was then turned upstream along the tunnel axis by a small mirror mounted in the airstream. The improvement in light intensity and distribution from the optical shroud was striking, both from visual observations and photographs. As hoped, the modulator gave good clean breaks in the streaks.

The first full-scale test of these new components of the illumination equipment was the RASA Support Test. A general photograph was presented in Fig. 5 previously. In Fig. 13 now, we see a closeup comparison between two pictures taken with and without lamp modulation. Both were shot at the same location, about 12 chord lengths downstream of the airfoil. The tunnel velocity was 50 fps and the airfoil was set at 10° angle of attack.

Fig. 13a shows the established tip vortex with its characteristic helical trajectories about a central core. The flow is from left to right, the lamp location lying slightly downstream to the right. Below the core, the streaks end abruptly because they pass out of the light beam. The most interesting feature is the difference between the trajectories above and below, or outboard and inboard, of the core. Inboard, the pitch of the helices increases, indicating that the axial velocity is less and the profile is not axisymmetric about the core. This must be a manifestation of the viscous wake behind the wing due to the boundary layer.

Fig. 13b depicts the same pattern photographed a few moments later with lamp modulation. A modulation frequency of 250 Hz was chosen here with 25% off-

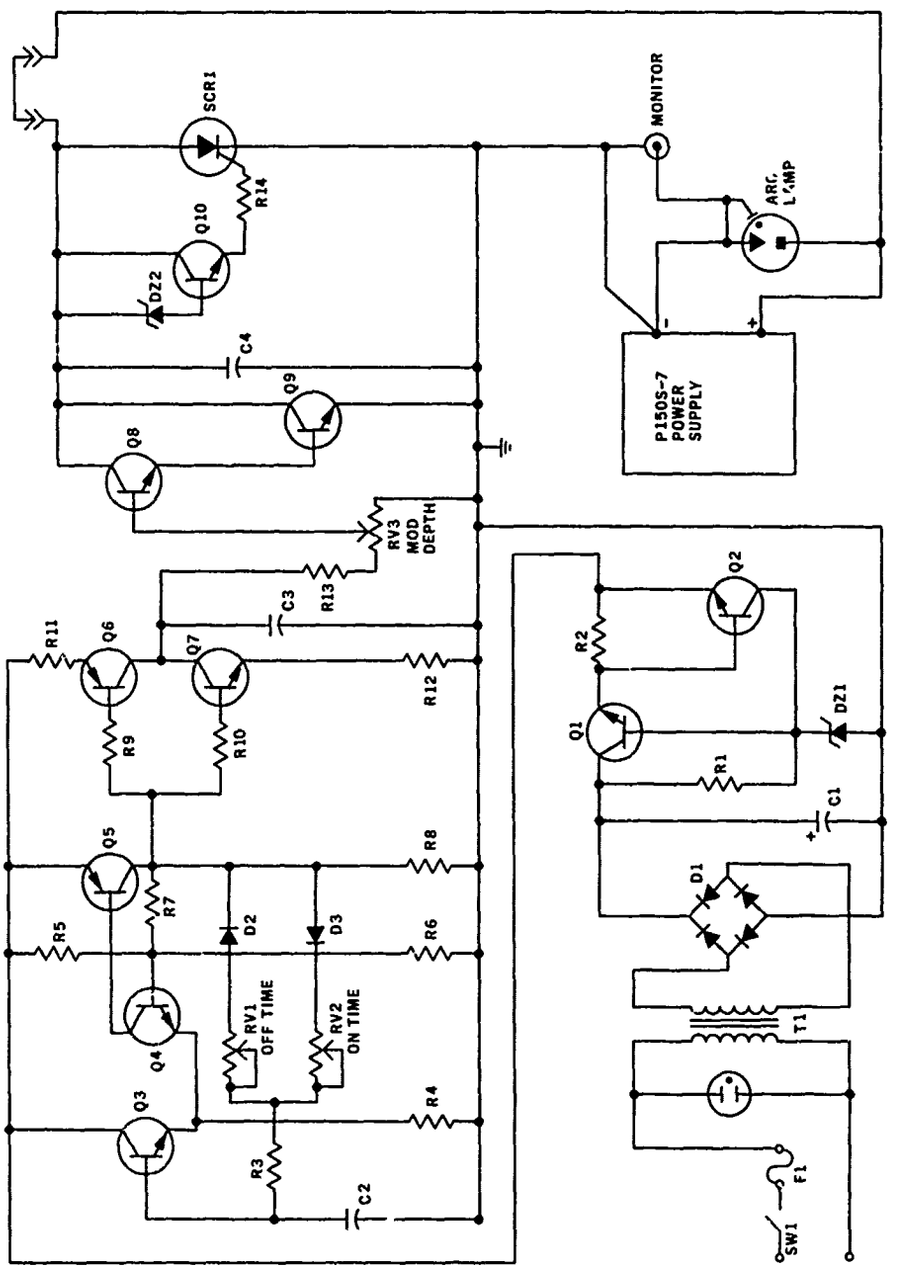

Figure 12. Diagram Of Modulator Circuit For Eimac Lamp Power Supply

Table 1. Modulator Parts List

Resistors

R1: 2.2 k, 1 w
R2: 2.5, 1 w
R3, R8: 470, 1/2 w
R4, R9, R10: 4.7 k, 1/2 w
R5, R6, R7: 22 k, 1/2 w
R11, R12: 4.7, 1/2 w
R13, R14: 1.0 k, 1/2 w
RV1, RV2: 100 k, 1/2 w Linear Taper Carbon Potentiometer
RV3: 10 k, 1/2 w Linear Taper Carbon Potentiometer

Capacitors

C1: 500 µf / 25 V Electrolytic
C2: 0.1 µf / 50 V
C3: 1.0 µf / 50 V
C4: 1.5 µf / 600 V

Diodes, Rectifiers

D1: HEP 175 Bridge Rectifier 50 V, 1.0 A d-c
D2, D3: HEP 154 Silicon Diode 50 V, 1.0 A
SCR1: HEP 306 Silicon Controlled Rectifier 15 A, 200 V
DZ1: HEP 606 Zener Diode 14 V, 1 w
DZ2: HEP 608 Zener Diode 27 V, 1 w

Transistors

Q1, Q10: HEP 243 Silicon NPN
Q2: HEP 50 Silicon NPN
Q3, Q4: HEP 736 Silicon NPN
Q5, Q6: HEP 51 Silicon PNP
Q7: HEP 53 Silicon NPN
Q8: HEP 701 Silicon NPN
Q9: HEP 704 Silicon NPN

Other Components

T1: Power Transformer
Primary: 115 V, 60 Hz
Secondary: 12.6 V @ 0.5 A
SW1: Switch, SPST 115 V, 0.2 A
F1: Fuse AGC 1/2
Neon Pilot Lamp: 115 V
Current Monitor Terminal: BNC Female

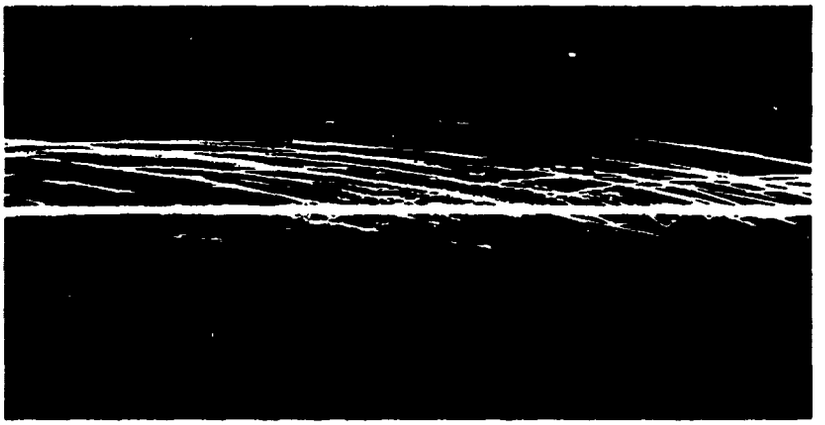

Figure 13a. Established Tip Vortex Flow Taken Without Modulation

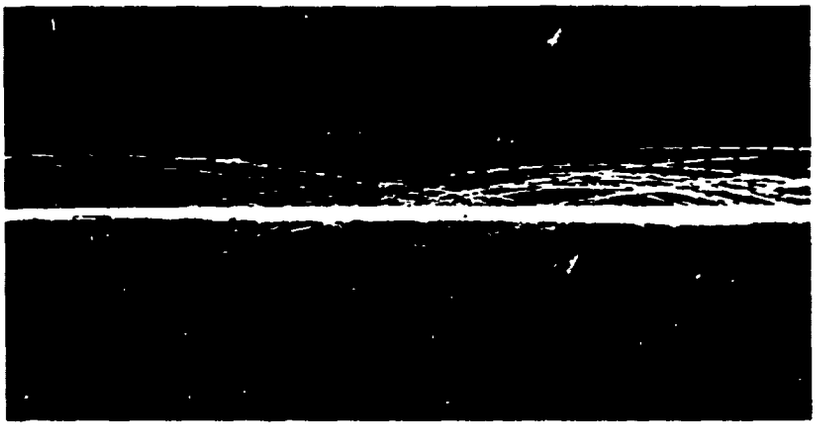

Figure 13b. Established Tip Vortex Flow Taken With Modulation

time. This meant that a bubble at the freestream velocity of 50 fps would go 0.2' or 2.4" between breaks in the streak. To compute the axial velocity component at various radii from the core, we simply determine the axial distance any bubble moves in one cycle relative to the distance a bubble in the undisturbed flow away from the vortex moves in one cycle. Since a bubble in the undisturbed flow moves at the tunnel velocity, the ratio of these distances times the tunnel velocity is equal to the axial velocity. We found that the axial velocities reach the freestream velocity just outboard of the core. Inboard, however, they are appreciably lower, averaging about 33 fps.

This is not all we can learn from this photograph. We computed the rotational and radial velocities as well. These are obtained by dividing the respective distances a bubble travels around and toward the core in one-half a rotation by the elapsed time. The elapsed time is the ratio of the number of cycles to the modulation frequency. Typically, the rotational velocity turned out to be about 15 fps and the radial velocity around 2 fps at a radius of 1.3". It would be very difficult to measure such a small radial component by any other method.

One other point should be mentioned. Not a great deal is known about the effects of modulation on the long-term performance of the arc lamp. After a period of modulation, the lamp intensity may change discontinuously by itself without external modulation. Fortunately, this malfunction disappears if the lamp is operated continuously for awhile. Although it has been the only problem, we suspect the lamp life is also shortened.

Despite our comments before, we should not neglect the role played by strobed lighting on the development of the high-speed head per se. Strobed lighting proved invaluable for viewing the bubbles as they were emitted from the head into the tunnel. This was the only way to establish whether the bubbles burst due to the turbulence or remained intact. We used an Ultra High Intensity Strobe manufactured by United States Scientific Instruments. It has a short-arc xenon lamp and is capable of flashing rates from 1 to 1,000 per sec. The light pulse duration varies from 1.25 to 7.0 μsec as the light intensity is increased over the available range. This unit provides a much greater intensity than other strobe designs and was very effective.

3.3 Photography

Photography serves as a means to record the bubble motions and thereby the air motion. This is particularly important at higher flow speeds when it becomes impossible to follow the bubble movement with the eye. Also, it is essential for making quantitative measurements of the bubble paths and flow velocities. Photography may not be the only way to accomplish this, but the techniques are highly developed and the equipment is readily available. Regardless, this area

was still a real challenge and demanded a lot of effort, plus some compromises.

We had to deal with two basic problems. The first problem is associated with the amount of light reflected by a bubble. This is equal to the intensity of the light falling on the bubble times the reflectivity of the bubble. The intensity depends upon the lamp itself and the distance from the lamp to the bubble. We have some control over these factors. The reflectivity, however, is our primary difficulty. Only two locations on the bubble film reflect light in the direction normal to the light beam and what is reflected, even at these points, is low. Consequently, of the total amount of light intercepted by a bubble, only a minute fraction comes out in the direction of the camera. We did attempt to increase the reflectivity by putting dyes into the bubble film, but the film is so thin that they had no noticeable effect.

The amount of light that actually exposes the film depends upon how fast the bubble is moving and the camera aperture. The bubble velocity in effect acts as a shutter so that if the velocity is doubled, for example, the film exposure at any point on the film over which the bubble image passes will be halved. As the camera aperture is opened, of course, more of the light from the bubble will enter the camera. This leads, though, to a reduction in depth-of-field.

Since the light intensities we have to work with are so low, we must employ fast, sensitive films. Higher lamp intensities are another answer but the cost becomes a factor. Also, this could lead to more background illumination and lower the bubble visibility.

Image size is the second basic problem. This is a problem because all we see of the bubbles are the two tiny highlights. The size of their images on the film depends on their size, which is proportional to the bubble size, plus the distance of the camera from the bubble and the film size. If we go to a larger camera, the image is correspondingly larger, but the choice of special films is limited to certain sizes. Secondarily, there is a very real convenience in working with roll film rather than sheet film for taking many photographs as rapidly as possible.

If the image size is too small, we fall below the resolving power of the film emulsion, which is a measure of a film's ability to record fine detail distinguishably. In this case, a group of bubble streaks no longer come out as individual lines on the negative, but as an indistinct gray mass. To aggravate matters, fast films characteristically have a low resolving power.

The sensitivity and contrast obtainable from any film is best evaluated from the film's characteristic curves. These curves are plots of the density of a negative as a function of exposure, each one associated with a particular developer, temperature and time of development. The curves are generally S-shaped with a toe, a rising straight portion and a shoulder. A fuller de-

scription is presented in Ref. 16. For our immediate purpose, we only need to point out the gross features of the film curves that we sought.

A fast film will have its characteristic curves starting at low exposure levels. For high contrast the straight portion must be steep. This can be enhanced by high-contrast developers and longer development times. Ideally, we would like the background exposure to fall below the toe of the curve and the bubble streak exposure to fall above, well up the rising portion. A steeper curve then produces denser bubble streaks for the same exposure. With the background below the toe, the remainder of the negative will be at the level of gross fog, or essentially clear. This ideal negative, on printing, will give sharp, bright bubble streaks on a black background.

This problem was discussed at some length with the Eastman Kodak Company. We had originally considered high-contrast film, high-speed recording film, high-speed color film and infrared film as possible candidates[1]. Kodak discouraged any effort with infrared and high-contrast film simply because they are too slow. This was already confirmed by some earlier experience. They did recommend we try color film and two types of recording film, Kodak 2475, which is available commercially in 35 mm magazines, and Kodak 2485, which is available only in bulk. With special development in each case, 2475 film has an exposure index of 3200 and 2485 film an exposure index of 8000.

Pursuing Kodak's recommendation, we did try high-speed color film in the SAI 6" x 6" Wind Tunnel. The color seemed to increase the contrast, but the film was inherently too slow for the higher tunnel velocities. The more complicated developing and printing, too, made it less appealing than the black-and-white recording films, particularly for in situ test shots.

We also tried the 2475 and 2485 films in our tunnel. Comparing streak photographs taken at various airspeeds up to 200 fps, we concluded that the extra work required for the 2485 film is not warranted. This extra work involved not only loading the film magazines from the bulk roll, but also developing the exposed roll with special developers at elevated temperatures.

As a result, 2475 film and a similar emulsion, Royal-X, was chosen for photography in the three test programs. The photographic and physical properties of 2475 film are listed in Ref. 17. This film comes in 16 mm, 35 mm and 70 mm rolls of different lengths. It also comes in a 36 exposure, 35 mm magazine. We used the 16 mm size in 125' rolls for motion picture photography in the third test program. The 35 mm magazines were employed for test shots and in the limited stereo work. The 70 mm size, of course, provides the largest negative and would have been best for the production visualization photographs. We did not have a 70 mm camera, though, so we turned to Royal-X film[16] instead for the bulk of the photography in the test programs. Royal-X can be purchased in

sheets and rolls. We picked 120-size rolls for convenience which gives a negative the same size as 70 mm film.

Since Royal-X and 2475 have similar emulsions, both films were processed with the same developer and development sequence. We experimented with several developers prior to the first test program, including Kodak D-19, DK-50 and Acufine. Taking Ref. 17 as a guide to development times, we felt that although the differences were not pronounced, D-19 produced the best contrast with a minimum of graininess. We adopted the processing sequence outlined with a development time of 12 min at 68°F. The total darkness required throughout was achieved with a small developing tank. Since the image-structure characteristics of the film become poorer with increasing temperature, the processing temperature was kept down. As recommended, we always mixed up fresh D-19 developer and acid stop bath to reduce the possibility of dichroic fog on the film.

Almost all of the photography was done with three cameras. The bulk of the still pictures were taken with a twin-lens Rolliflex which has a 2 1/4" square frame size. Occasionally, we backed up some of our still pictures with a single-lens 35 mm Miranda Sensorex. Both of these cameras were owned in-house. For the movies we rented a 16 mm Bolex H16 equipped with 16, 25, 50, 75, 100 and 150 mm lenses. The longer focal-length lenses were especially useful to enlarge the bubble images. Otherwise, with the frames so small, the streaks fall below the resolution of the emulsion.

For the combination of cameras, film and lighting employed, the exposures became essentially a function only of the tunnel velocity. Judged upon the quality of the streak image density, contrast and resolution, a camera aperture of $f/4$ at V = 50 fps worked well in most test shots. Correspondingly, we had to open up one stop to $f/2.8$ at V = 100 fps. These low f-numbers were somewhat disappointing, especially when we wanted more depth-of-field than we had. As a consequence, we took most of our photographs at 50 fps.

The high bubble generation rate permitted fairly fast shutter speeds. We found that 1/10, 1/5 and 1/2 sec gave us a good range in the number of streaks captured in a photograph. As pointed out previously, these fast speeds helped greatly to reduce the exposure of the stationary background.

Making prints or enlargements from these negatives requires some experience. Ideally, the negatives should have dense, continuous and fairly wide streaks on a clear background. If this is so, we can get bright white streaks on a completely dark background with a high-contrast paper. Often, though, the streaks are not as dense or uniform as needed. If this is enlarged onto high-contrast paper, the white streaks seem ragged and uneven. It is better, then, to try a lower-contrast paper and vary the exposure time.

Let us turn now to some specific photographs from the test programs. The pictures with the best photographic quality were obtained during the first test at the NAE. Printed on high-contrast paper, the bubble streaks are exceptionally clear. The principal reason for the superior quality is simply that we were closer to the bubbles than in the later tests, ranging from 14" to 40" away. At such a close distance, the wider streak image was sufficient, with the amount of light reflected from the bubbles, to give good resolution. Besides, the streak/background contrast was the highest in this test, further favoring the resolution. So.. : grain still exists in the negative, but this essentially disappears into the background in the print.

The quality of these pictures was shown in Figs. 3 and 4. Two other examples are presented in Fig. 14. These demonstrate the effect of different shutter speeds. Fig. 14a was taken with a shutter speed of 1/2 sec. While we can see the overall pattern beautifully, it is hard to follow an individual streak very far. Fig. 14b, on the other hand, was taken at a shutter speed of 1/10 sec and the reverse is true. In both cases the freestream velocity was 50 fps and the angle of attack was 0°. There are two other things to note. The variation in the streak brightness due to the nonuniformity of the lamp beam is quite evident. Moreover, the small depth-of-field which is caused by the low f-number can be detected readily, some of the streaks being a little out of focus.

The best quality photographs from the later tests are the downstream shots of the tip vortex in the RASA Support Tests. Two examples were just seen in Fig. 13. Here we were slightly farther away, about 5', but we had the advantage of more light since the lamp was immediately downstream of the bubbles. These streaks were bright enough to print on high-contrast paper. To photograph the tip vortex right behind the blade, we had to aim upstream so the camera was about 6' to 7' away. More important, though, the lamp was 16' downstream of the blade, weakening the intensity markedly. The streaks are much thinner and less dense as a result and we were forced to go to lower contrast paper in printing.

The photographs from the last test program are of about the same quality. We would expect this because the lamp was about the same distance from the blade and we photographed at distances between 4' and 8'. Accordingly, we had to take more care in printing. Some examples of these pictures will be introduced shortly.

A modest effort on stereo still photographs was undertaken, too, on the last test program. However, the results were not very satisfactory, mainly due to our camera limitations. The camera was a Sawyer's fixed-focus model. It takes a pair of negatives that are only about 1/2" square. We used the two lowest settings, f/3.5 and f/4, and placed the camera as close to the bubbles as pos-

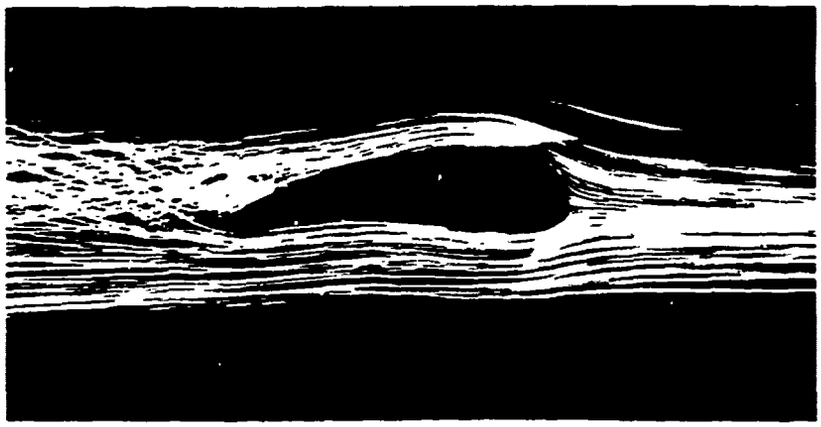

Figure 14a. Photograph Of Airfoil Flow Pattern Taken At 1/2 Sec

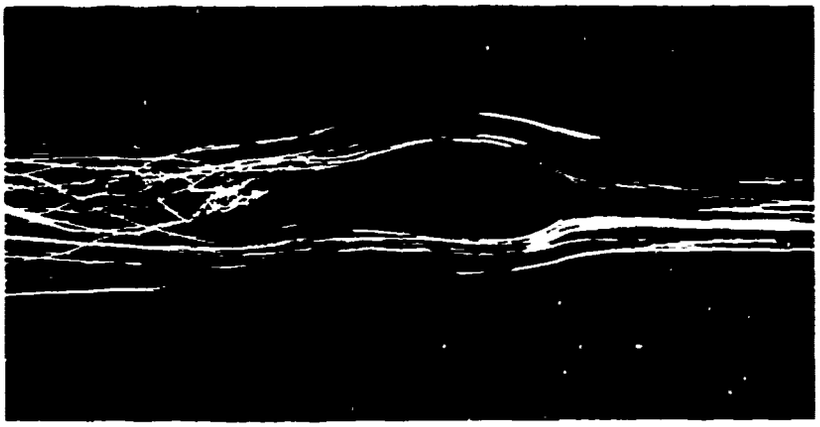

Figure 14b. Photograph Of Airfoil Flow Pattern Taken At 1/10 Sec

sible, approximately 5' away. The lighting was the same as for the other still pictures. Disappointingly, the negatives were extremely thin with only a few, very faint streaks. We attributed this to the limited negative size which brought the streak images down to the resolution limit of the film emulsion.

There is no reason why stereo photography will not work equally as well as conventional still photography. Furthermore, we feel it can be a real asset for interpreting three-dimensional flow patterns. A larger frame size is what we need mostly unless the light levels can be raised considerably. There are a number of commercial stereo cameras on the market which take a full 35 mm stereo pair. To go to still larger sizes, we might be able to synchronize a pair of cameras.

Our attempt to take motion pictures was more successful. Although the 16 mm frame size is even smaller than the stereo, we had the advantage of the closeup lenses. This got us above the resolution limit of the film by enlarging the streak images. Also, we had the advantage of lower f-numbers to increase the amount of light reaching the film.

We took all of the movies in real time at a speed of 24 frames/sec. From the 500' of film exposed, we selected 8 sequences, or about 125', to print and project. Three of these sequences were made from the side of the tunnel with the camera 7' to 8' away from the bubbles. For this location the 50 mm lens at $f/2$ was fine. Two of the other sequences were shot from above, 3.5' away. We used a 16 mm lens at $f/2$ and a 50 mm lens at $f/2.8$ here. The remaining three sequences were taken from inside the tunnel diffuser, looking upstream with the tunnel running at a slightly lower velocity of 34 fps. To get the coverage we wanted, we went to the 25 mm lens at $f/2.8$. In these last sequences, the streaks run in and out of focus because of the upstream angle of view and the low f-number.

Through special processing, it was possible to develop this movie film in essentially the same manner as the still pictures with D-19 developer. Since 2475 is a negative film, it had to be printed, too, but we were unable to experiment with high-contrast print stock. Instead, we printed the edited sequences on 7302 film, Eastman Fine Grain Release Positive, with development in D-16, a fine grain sound film developer.

This print, when projected, is not as high in photographic quality as our still enlargements. The streaks are more ragged and less bright, while the background is not dark enough to hide the grain from the negative. The results might be improved considerably just by printing on high-contrast stock with special development. Nevertheless, the image is enlarged enormously when projected so we really need an exceptionally sharp print to match our other pictures.

We feel, despite this, that our initial attempt at motion photography of the bubbles was a real success. Without question, it shows quite realistically what is seen by the eye, except without the same clarity. From the sequences of the flow as the blade rotated through a range in angle of attack, the build-up and subsequent breakdown of the tip vortex that was recorded is most dramatic and, to our knowledge, unique. Clearly, we have gained access to new information by this means that should be especially important in analyzing unsteady flows.

In future work, the picture quality could be upgraded significantly by shooting with 35 mm film and then making a reduction print onto 16 mm film. This would get us further from the resolution limit of the emulsion, giving denser and sharper images, and reduce the grain. We should also experiment with high-contrast print stocks as a way to heighten the streak brightness and reduce the grain even more.

As we discussed much earlier, we did take some high-speed motion pictures during our first test program at the NAE. These were made with a Milliken camera at 500 frames/sec. Though the results were rather marginal, it may be necessary to go to these higher framing speeds when the fluctuations or pulse rate of an unsteady flow are high enough. The same suggestions for better picture quality would apply in this case as well.

Finally, we should mention the application of video tape to motion photography of the bubbles. This avoids a film with its emulsion characteristics and limitations entirely! Other apparent advantages include the fact that we can intensify the bubble images electronically and that we can replay them instantly, thereby eliminating the time-consuming developing and printing procedures. Undoubtedly, it has disadvantages, too, not the least of which is the time and spatial resolution associated with the scanning rate of the vidicon tube and the number of lines scanned.

To explore the potential of this method as a visualization tool, we conducted a brief in-house test with a commercial Sony ACV-3200 Video Camera / AV-5000A Recorder. What we recorded was the visualization of the flow about a circular cylinder in the test section of the SAI 6" x 6" Wind Tunnel. The tape was very encouraging. At speeds up to 50 fps, the bubble streak images on a TV monitor were bright and relatively sharp. More impressive, though, was the ability to look at the recorded flow pattern immediately afterwards. We were able to do this both in real time and "frame-by-frame". There is no doubt in our minds that this approach should be explored further.

4 EVALUATION OF THE SYSTEM

4.1 Present Capabilities

An important aspect of this work was to try to enlarge the speed range over which the visualization system can be employed successfully. The upper limit on wind tunnel velocity is determined by three principal factors. First is the limit at which bubbles can be implanted in the flow by the head without bursting. Second is the limit of the accuracy with which bubbles can trace a particular flow pattern. Third is the limit imposed by the ability to create good photographic records of the bubble paths with the equipment at hand. The question of accuracy will be discussed later. For the moment, we will concentrate on the capabilities of the head designs and the photographic/lighting scheme.

Based on the tests carried out in the SAI and NAE wind tunnels, we have established that bubbles can be implanted at speeds at least as high as 200 fps with either the prototype or modified high-speed heads. This can be done without the aid of a sunburst section when the newly-developed bubble film solution is used. Between the two heads, we prefer the prototype high-speed head because of its smaller size.

Further tests at higher tunnel velocities will be necessary to determine the actual speed limits for the two heads. Various combinations of sunburst sections and shroud lengths should be tried. We expect that the highest speed can be reached with the larger, modified head, incorporating the sunburst section and a somewhat longer contracting shroud than we chose for our first test program at the NAE.

The part of the system which most severely limits us at the present time is the photography/lighting. The bubbles simply do not reflect enough light to allow us to photograph the trajectories they trace at the higher velocities, say 100 fps and up. This means that either the incident light must be increased or the bubble reflectivity improved. A brighter light is the easier remedy, provided it does not become too bulky or reduce the contrast between the bubble streaks and the background too much. More light could be produced with a larger lamp, such as one of those described earlier. An alternative solution is to go to several of the 150-watt arc lamps.

The opportunity for real improvement, though, lies in the bubble reflectivity because it is so low. We experimented to some extent with additives to the bubble film, such as dyes, and to the interior gas, such as smoke. These did not help significantly. Still, more effort should be made along these lines. The main difficulty lies in the fact that the bubble film is extremely thin,

say typically 0.5 μ.

We cannot expect to improve the photography through more sensitive film emulsions. We are now using very fast films which have relatively coarse granularity and moderately low resolving power. These image-structure characteristics would become even poorer with faster films. Actually, we would prefer to go in the other direction, to slower films, for better image structure if the bubble streaks could be made brighter.

When the visualization system is employed in a large-scale subsonic tunnel, like either of the 8' x 10' tunnels at NSRDC, the camera is generally 4' to 8' away from the bubbles. Under these conditions we have to open up to settings of f/4 and f/2.8 at tunnel velocities of 50 and 100 fps, respectively, to obtain good photographs. Since lenses on large format cameras are rarely faster than f/2.8, 100 fps represents a rough photographic limit at the present time. If the image size can be increased by moving the camera closer, we can probably gain one f-stop and get up to 200 fps tunnel speed. We actually recorded bubble streaks at 200 fps in the NAE test program by placing the camera much nearer. The low f-numbers, however, create a depth-of-field problem at short range.

The problem of streak resolution and sharpness, then, is what determines the maximum velocity at which good streak pictures can be made in a given size tunnel. For a very large tunnel, we would recommend an electrically-driven camera. The camera could be positioned inside the tunnel in the region of interest and operated remotely from the outside.

The considerations for a small wind tunnel are mainly the head size and its wake, since the test section is generally not too long. In the event that the blockage and wake are problems, the head can be located upstream in the settling chamber of the tunnel, just downstream of any damping screens. Particular care must be taken with respect to any possible influence on separation.

As mentioned earlier, the bubbles spread out to cover a region about 5" in diameter 10' downstream with a single head. This spreading is due to the tunnel turbulence and the amount is typical of the tunnels we employed in our test programs. For coverage of a larger region, multiple heads can be mounted upstream, spaced to give an even distribution of bubbles. We have constructed a divider unit which can drive up to three heads from a single console. This approach is essential in the case of an unsteady flow. If, on the other hand, the flow is steady, one head can be positioned at different locations. We tried this in the Kármán-Trefftz airfoil test, taking multiple exposures on a single photograph with the head at different elevations for each exposure. The results were very satisfactory.

One more point we should discuss briefly is the capability of making velocity measurements with this technique. The modulator we designed can cycle the lamp at frequencies from 100 to 10,000 Hz. We picked a frequency of 250 Hz for most of our modulated photographs taken at a tunnel velocity of 50 fps. At this velocity, a bubble in the freestream travels 0.2' or 2.4" during each cycle. To maintain a distance of 2.4" of travel at lower velocities, the frequency has to be reduced. The lowest velocity we can go down to is 20 fps at 100 Hz. At the other extreme, the highest velocity that 10,000 Hz will take us is 2000 fps, well past the present capabilities of the head and photography.

From a single photograph we can measure only the two velocity components that lie in the plane of the photograph. To get the third velocity component normal to these components in a three-dimensional flow, a second camera is necessary. These two cameras should be synchronized in order to capture the same bubble trajectories. If the flowfield is axisymmetric, photography from a single direction may be sufficient by taking the symmetry into account in the data reduction. We used this approach in calculating all three velocity components within the tip vortex from Fig. 13b.

4.2 Accuracy

As a bubble is carried through a nonuniform flowfield, it experiences some motion relative to the air surrounding it whenever the air mass changes velocity and direction. This relative motion produces an aerodynamic force, or drag, on the bubble which accelerates it to the new velocity and direction. How rapidly the bubble can respond to these changes and how fast these changes take place determines how faithfully the bubble will trace out the actual air motion.

To find the answers, we will draw first on the extensive work with airborne particles, or aerosols, for some basic principles. Then, we will apply these principles to the case of neutrally-buoyant bubbles and interpret the results from our investigation of accuracy in the Kármán-Trefftz airfoil test.

The drag force exerted on any particle imbedded in an arbitrary flow, due to relative motion between the two, cannot be predicted in general. The problem is exceedingly complex. As a starting point in the study of the motion of airborne aerosol particles, an approximate drag force expression is applied. This expression was derived almost a century ago by A. B. Basset and J. V. Boussinesq, and later by C. W. Oseen, based on a model in which a sphere travels in a straight line through a stationary, viscous fluid. The sphere velocity, or Reynolds number, is taken to be so small that the inertia terms in the Navier-Stokes equations can be neglected, as in the classical Stokes and Oseen approximations. On the other hand, the sphere can have an arbitrary acceleration.

The approximate drag force has three terms[18,19]. The first term is proportional to the instantaneous sphere velocity, coinciding identically with the Stokes drag law. The second term is proportional to the instantaneous sphere acceleration. It is independent of the fluid viscosity and is equal to the added-mass force calculated for a sphere accelerating in a potential flow. The third term is a complicated integral over the acceleration history which accounts for the force arising from fluid motion created by the earlier movement of the sphere.

Of these three terms, the second term can be dropped immediately. That is, the added-mass contribution is equal to half the corresponding sphere volume of air times the particle acceleration. If the ratio of the fluid density to the particle density is very small, as it is for aerosol particles in air, this contribution is negligible.

The magnitude of the third term, or integral term, cannot be assessed so easily. Calculations of its effect, though, have been carried out for several specific cases[18]. The results show that it, too, depends upon the ratio of the fluid density to the particle density in these cases and may be discarded. Therefore, the drag on the particle at any instant can be considered to be the same as it would experience at a constant velocity equal to the instantaneous velocity.

Strictly speaking, this simplified drag force applies only to motion along a straight line. If we adopt it for motion along any path, a number of important relationships can be derived. The first concerns the relaxation time,

$$\tau = m / 6\pi\mu r \tag{1}$$

where m and r are the particle mass and radius, respectively, and μ is the fluid viscosity. In terms of τ, the equation of motion for the particle becomes

$$d\underline{U}_p/dt = (\underline{U}_f - \underline{U}_p) / \tau \tag{2}$$

neglecting any external forces, including gravity. The vector $\underline{U}_p$ is the velocity vector of the particle and $\underline{U}_f$, of the surrounding fluid. Clearly, τ has the units of time. It depends solely on the particle size and mass, assuming that the fluid is always air.

If we apply Eq. (2) to the case of a particle having a given initial velocity in a stationary fluid, we find that the particle slows down to $1/e$ of this initial velocity at $t = \tau$. From this we see that τ is a relaxation time in the sense that it is a measure of the time required for a particle to "respond" to

any velocity vector difference ($\underline{U}_f - \underline{U}_p$) and take on a new fluid velocity and direction. When τ is small compared to the characteristic time over which $\underline{U}_f$ changes, the particle should follow this change accurately.

To quantify this last idea, the Stokes number is introduced as a similarity parameter. Consider a particle-laden airflow past an obstacle of dimension D. If the flow velocity away from the obstacle is U_o, we can make the velocities in Eq. (2) dimensionless by dividing each side by U_o. Similarly, we can make the time dimensionless by dividing it by D/U_o, which is the time for the flow to travel past the obstacle. Denoting the dimensionless variables by primes, we can rewrite Eq. (2) as

$$d\underline{U}_p'/dt' = (D/\tau U_o)(\underline{U}_f' - \underline{U}_p') \qquad (3)$$

The quantity $(\tau U_o/D)$ is dimensionless. It is called the Stokes number[18]. Expressed in the form $\tau/(D/U_o)$, we see that the Stokes number is just the ratio mentioned above, that is, the relaxation time divided by the characteristic time of the flow.

Eq. (3) indicates that once $\underline{U}_f'$ is known for a steady flow around an obstacle, the particle trajectories depend only upon the Stokes number. The fluid flowfield, and therefore $\underline{U}_f'$, is determined in turn by the Reynolds number $U_o D/\nu$, where ν is the kinematic viscosity of the fluid. Consequently, the paths of the particles about an obstacle of any chosen shape, made dimensionless by D, are a function, in general, of both the Stokes and Reynolds numbers. If the ratio of particle density to fluid density is fixed, then the paths will be a function of the Stokes number and the ratio r/D.

In the study of the deposition of aerosol particles on objects, a collection efficiency is introduced[18] which is essentially an inverse accuracy parameter. The collection efficiency is defined as the number of particles actually deposited on the object over the number which would be intercepted if all of the particles moved in straight lines without any aerodynamic effect at all. When the collection efficiency vanishes, all of the particles are swept around the object and follow the air motion accurately.

From our above discussion, the collection efficiency of an object of a given shape depends principally on the Stokes number. It also depends on the Reynolds number, or r/D alternatively, if the flowfield changes appreciably over the range of U_o and D considered. The collection efficiency increases with increasing Stokes number, that is, with increasing τ and U_o and decreasing D. We see this effect in nature, for example, in the icing of wires, poles and trees by a wind-driven rain or fog. Since $\tau \sim m/r \sim r^2$, icing becomes more severe the droplets become bigger and/or the wind speed increases. On the

other hand, smaller branches and wires collect ice more rapidly than the larger branches and poles.

A great deal of experimental data on collection efficiency for cylinders and spheres is presented in Ref. 18. The Stokes number appears to correlate these data quite well. The collection efficiency is 0 up to a Stokes number on the order of 0.1. This value is called the critical Stokes number. Above 0.1, the curve is S-shaped and reaches a value near 1 when the Stokes number becomes on the order of 100. Some theoretical calculations based on Eq. (3) are in substantial agreement.

With this background, let us now turn to the question of accuracy in tracing flows with neutrally-buoyant bubbles. In this case, our "particle" has the same density as the fluid and the simplifications made for aerosols must be reexamined. The added-mass term can be retained easily in the equation of motion, but the integral term would add a great deal of complication. In order to retain the concept of a relaxation time and a Stokes number correlation, we must ignore the integral term. If we do this, the relaxation time becomes just

$$\tau = r^2/3\nu \qquad (4)$$

or 1.5 times the value[18] of an aerosol particle because of the added-mass effect. Here, r is the bubble radius and ν is the kinematic viscosity of air.

It might be possible to explore the relative importance of the integral term analytically for motion along a straight line following Ref. 18, but we could only approximate the solution for the motion along any other path. Instead, we chose to investigate the problem experimentally. The idea was to visualize a steady flowfield where the streamlines could be calculated to a good approximation. From comparison of the bubble paths with the predicted streamlines, we would be able then to assess the accuracy.

The Kármán-Trefftz airfoil selected was described earlier. We developed a computer program to plot the airfoil and the streamlines about it from potential flow theory. For the test, an angle of attack of -5° and a tunnel speed of 100 fps were picked to minimize the viscous effect of the boundary layer and separation.

A comparison between the computed flowfield and one of the streak photographs is depicted in Fig. 15. The airfoil drawn by the computer appears smaller than the one in the photograph since we tried to match the airfoil size at the lateral position of the head, 6" in from the window, where most of the bubbles passed by. As noted earlier, the crossing of the bubble paths indicates that the tunnel flow was not completely steady. Still, we can make out a mean flow pattern quite easily. There is a slight separation of the flow near the

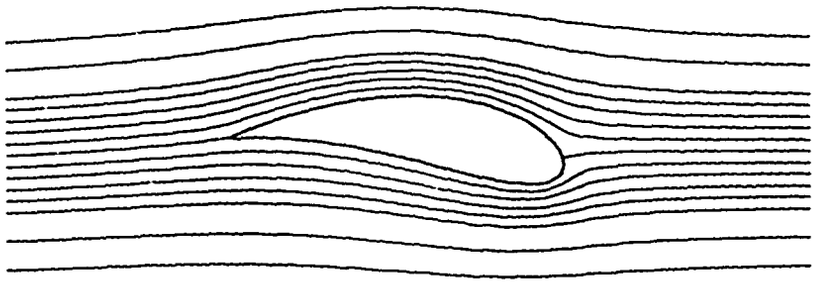

Figure 15a. Streamlines Of Potential Flowfield For 2-D Kármán-Trefftz Airfoil

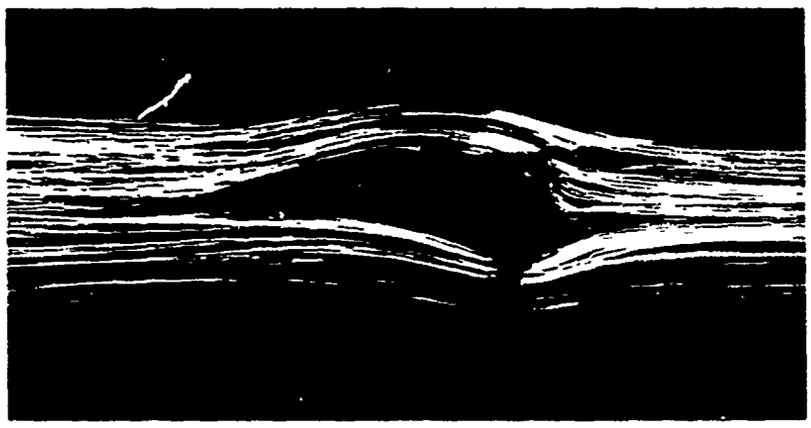

Figure 15b. Comparative Streak Photog aph From Wind Tunnel Test

trailing edge but it is very small compared to the separation we saw in Figs. 3 and 4.

The agreement between the two flowfields, overall, is extremely good. The most difficult portion of the flowfield for the bubbles to follow is in the stagnation region because the gradients are the steepest. While we cannot see right to the stagnation point, the bubbles which approach close to the stagnation streamline turn very nicely and curve around the airfoil. Near the trailing edge, the separation region appears to produce a flattening of the bubble paths that is absent in the theoretical flowfield. In contrast, though, the streamline curvature above and below the airfoil is somewhat greater. This is the opposite of what we would expect from Eq. (3) if τ were too large. That is, the bubbles approaching along and near the stagnation streamline would impact on the airfoil while those farther away should follow flatter trajectories than the streamlines.

From Eq. (4), the calculated value of τ for the bubbles is 0.057 sec. To determine a Stokes number, let us set D equal to half the thickness of the airfoil so that we can compare with the data in Ref. 18 for circular cylinders. Then, $(\tau U_o/D) = 76$, taking $U_o = 100$ fps and $D = 0.9"$. At this value of the Stokes number, a circular cylinder immersed in a flow of suspended aerosol particles has a collection efficiency of almost 1, so that the particles should not follow the flow well at all. Clearly, this inconsistency means we need to know more about the aerodynamic forces on the bubbles.

Along these lines, some experiments are reported in Ref. 20 on both neutrally-buoyant bubbles and balls in air and water, respectively. It was found that the effective drag during acceleration was much higher than the steady state drag. Furthermore, although the relative Reynolds numbers were well above 1, the drag coefficient was found to vary inversely with the Reynolds number, as the Stokes drag, with the coefficient over 100 times higher than the Stokes value. Since τ is inversely proportional to the drag, in general, the Stokes number in our case would be reduced correspondingly to something less than 0.76. For circular cylinders at this Stokes number, the collection efficiency is very low and the accuracy is quite good. We would expect it to be even better for the airfoil shape. Thus, we may have a partial explanation to the apparent inconsistency.

We do not know now why the drag should be so much higher. This question certainly requires further investigation. More directly, however, we should resolve whether we can use the Stokes number as a correlation parameter for flow tracing accuracy or not. If we can, we would have a relatively simple way to gauge the visualization accuracy for a test, a priori. Meanwhile, we suggest that it serve only as a guide by comparison with the Stokes number for tests on similarly-shaped models where the visualization accuracy has been demonstrated.

4.3 Effectiveness In A Support Role

In a typical aerodynamic test program, forces, pressures and velocities are measured with various types of instrumentation. Flow visualization can play an important role in supporting these measurements by providing a clear picture immediately of the flowfield and its interaction with the model. We will begin with certain aspects of this support which would apply to any test and then give some specific illustrations from the RASA Support Test.

During the initial phase of a program, flow visualization should be used to examine the overall flowfield about the model and to search for unforeseen problems. Such problems, for example, might include undesirable interference with the tunnel or instrumentation, time-dependent effects or regions of turbulence, or poor simulation of a two-dimensional flow pattern. Corrective steps, as required, can be made and quickly rechecked with flow visualization. This procedure saves considerable effort compared to mapping out the flowfield by means of a tedious, point-by-point series of probe measurements.

After production testing starts, visualization will reveal at once any global changes in the flowfield produced by varying the test parameters. In turn, for a chosen set of parameters, it can locate regions of interest in which detailed probe measurements are desired. As a result, visualization serves to minimize the time needed to gather quantitative data.

Finally, flow visualization can be very important in the interpretation of data. This is especially true when the flowfield is a complex three-dimensional one or if there are appreciable unsteady effects. It will also show up small velocity components that might escape detection in the probe data.

Turning now to the RASA Support Test, flow visualization with neutrally-buoyant bubbles played a key role in three ways. First, it located the vortex when the tuft grid proved ineffective. Second, it identified the vortex characteristics, particularly the core size. Third, it showed dramatically how the vortex responded to the air jet emanating from the blade tip.

The effectiveness of the flow visualization in showing the results of blowing is demonstrated in Fig. 16. These two photographs were made right after the photograph in Fig. 5, taken with no blowing. The tunnel velocity was 50 fps and the blade was set at an angle of attack of 10° in each case.

In Fig. 16a, the injected mass flow rate was 0.014 lb/sec. This gave a mean jet velocity of 88 fps, or about 1.8 times the tunnel velocity. Here we see that the trailing vortex has changed considerably, but a somewhat ordered structure to the flow persists. That is, the lower concentration of streaks appears to have a core-like structure about which remains a considerable amount of rotation. This was confirmed by the photographs taken from overhead. On

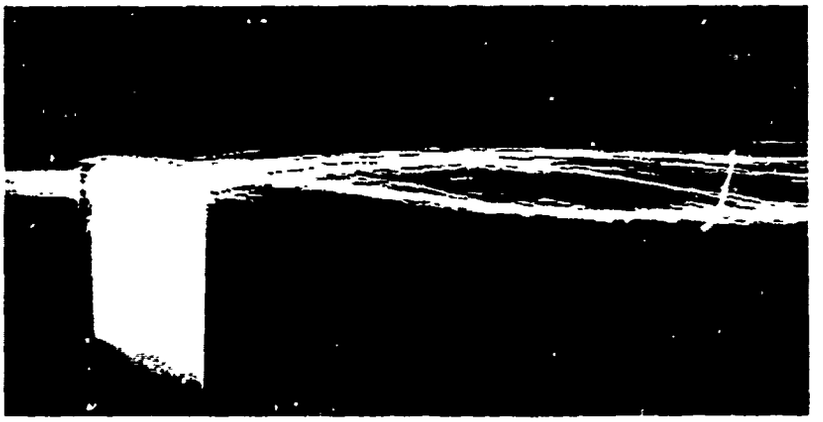

Figure 16a. Structure Of Wake Near Blade Tip With Low Blowing Rate

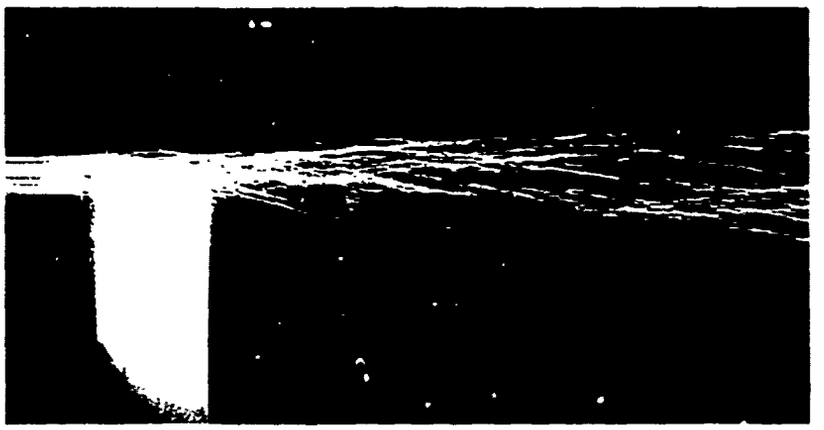

Figure 16b. Structure Of Wake Near Blade Tip With High Blowing Rate

the other hand, at 12 chord lengths downstream, we found that the trailing vortex is virtually the same as without blowing.

In Fig. 16b, the injected mass flow rate was increased to 0.034 lb/sec, raising the mean jet velocity to 214 fps, or over 4.2 times the tunnel velocity. The flow just downstream of the tip now seems almost completely random and turbulent, with no evidence of a vortex structure. We can not identify a distinct core in our photographs farther downstream either, but a general rotation emerges. Whether this apparent reforming process continues or not requires additional investigation.

4.4 Potential As An Investigative Tool

The third test program was really our first opportunity to evaluate the flow visualization technique as an investigative tool. In this program, the HR2S-1 blade tip model was large enough so that we could record details of the tip vortex formation which were not evident in the previous test. As far as we know, the photographs we took are unique in this regard.

In order to illustrate how the visualization can provide basic information, we will examine and interpret several representative photographs from the test. At the same time, we will compare our observations with two other results. These results were obtained recently by the NASA from a comprehensive hot wire survey[21] and by the FAA from full-scale tests[22].

Shown in Fig. 17 are two different views of the bubble traces passing over the HR2S-1 blade tip. In Fig. 17a, the view is from the side of the wind tunnel about 5' to 6' away, looking directly at the plan view of the upper, or suction, surface. In Fig. 17b, the view is from overhead but only 3' to 4' away, looking endwise at the blade tip. The trailing portion of the tip appears as a bright spot at the left. The leading edge is in the shadow at the right, near the point where the lowest bubble streaks begin. The chord line of the airfoil follows along the shadow line emanating from the bright spot at the trailing edge. In both photographs, the flow is from right to left with a freestream velocity of 50 fps. The blade angle of attack is 8°.

The predominant feature of the flow is the rapid spiralling of the bubbles into a growing core. The rate of entrainment is remarkable, with many of the bubbles reaching the core in one rotation after coming over the tip. Just the bubbles that come in farthest from the tip, or around the leading edge, have not entered the core by the time they reach the trailing edge of the blade.

We can get a quantitative measure of this entrainment by counting the number of streaks outside the core at the trailing edge. Since the flow pattern and bubble generation rate are essentially steady over the duration of the expo-

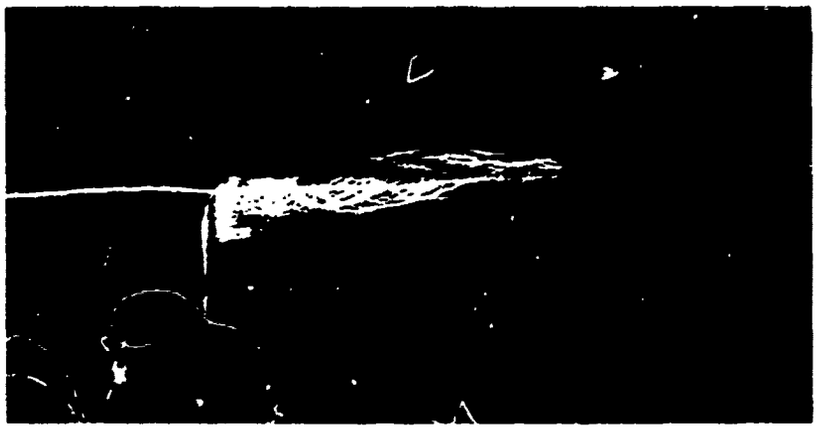

Figure 17a. Tip Vortex Formation On HR2S-1 Blade, Plan View Of Upper Surface

Figure 17b. Tip Vortex Formation On HR2S-1 Blade, Viewed Endwise Much Closer

sure, the total number of streaks at all axial stations must be the same. Consequently, the total number of streaks can be counted arywhere that they are distinct. In Fig. 17b, the best location is just upstream of the formation of the vortex core. Taking this total number minus the streaks outside the core at the trailing edge gives the number of streaks which make up the core there. From Fig. 17b, we found that about half of the bubbles have entered the core by the time they reach the trailing edge! The rest of them spiral in farther downstream.

Such rapid entrainment would lead us to expect an axial velocity in the core appreciably above the freestream velocity. This conclusion is borne out by the results of Chigier and Corsiglia[21]. In the vortex core at the trailing edge, they measured a peak axial velocity 27% above the freestream velocity.

Before we go ahead, we should clarify what we mean by the vortex core. The bubbles spiral into a tubular region so small that the individual streaks blend together to create a single bright band in the photographs. This band defines a "sub-core" that carries the entrained air. The radius of this sub-core is less than the usual core radius judging from the steep pitch of the bubble traces outside the sub-core. The usual core radius is defined as the radius at which the rotational velocity reaches a maximum.

From Fig. 17a, we see that our sub-core gets bigger up to about the trailing edge, but does not grow noticeably thereafter. The radius at the trailing edge is equal to 0.6% of the blade chord. The correlation equation for the vortex core radius in Ref. 22 predicts a value of 1.7% of the blade chord, or about three times the radius of the observed sub-core. This seems very reasonable. The results of Ref. 21, however, give a value of 7.7%.

The sub-core serves to locate the axis of the vortex. The vortex starts somewhere near the leading edge of the blade. It goes almost straight back to the trailing edge, moving inboard slightly in the plan view. Viewed endwise, the axis makes an angle of 4° with the blade chord line. This is half of the blade angle of attack. At the trailing edge, the distance of the center of the core from the trailing edge divided by the blade span is the same as measured in Ref. 21. The trajectory upstream and downstream is different, though. We attribute this difference principally to the fact that the NASA airfoil had a square tip. Also, their blade was 15% thick rather than 10% and it was set at an angle of attack of 12°.

One interesting feature of the vortex is the presence of "kinks" in the vicinity of the trailing edge. There are two kinks in Fig. 17a, the vortex bending further inboard downstream of the second kink. In Fig. 17b, we have only one kink. This seems to coincide with the first kink that is seen in Fig. 17a.

A perspective view of the tip vortex is presented in Fig. 18 which clearly portrays the three-dimensional nature of the phenomena. This photograph was taken at 1/4 and 1/5 sec with the camera inside the tunnel diffuser facing up-

Figure 18. Perspective View Of HR2S-1 Blade Tip Vortex

stream. The tunnel velocity was 34 fps. Due to the viewing angle, the streaks at either end are out of focus. The large apparent diameter of the core downstream was produced by a slight wandering of the vortex. It turns out that the tip vortex is very sensitive to disturbances in the tunnel. In this case, there were two people with the camera who moved slightly during the exposure.

This photograph shows more strikingly the entrainment of bubbles into the core and the helical path of the bubbles outside the core. Note again that a substantial fraction of the bubbles coming over and around the blade tip are in the core immediately downstream of the trailing edge. Almost all of the remaining bubbles spiral into the core within the distance downstream spanned by the photograph. Certainly, the radial inflow must be an integral part of the mechanism which sustains the vortex strength for miles behind large aircraft[22].

CONCLUSIONS AND RECOMMENDATIONS

An investigation was conducted to improve the technique for flow visualization with small, neutrally-buoyant bubbles and to assess its performance. Emphasis was placed on implantation of bubbles at higher airspeeds, integration of the various elements into a flow visualization system and evaluation of the system performance by means of a series of wind tunnel tests. The most important conclusions and recommendations are:

Flow visualization with bubbles is a unique and readily applicable technique for tracing particle paths and measuring velocities in steady or unsteady, laminar or turbulent airflows.

The integrated system has been completely qualified for wind tunnel testing at moderate subsonic speeds, either in a support role or as an investigative tool on its own. It is practical, economical and easily adapted to different problems. Furthermore, the equipment can be set up very quickly without any special wind tunnel arrangements. Contamination of the airflow or wind tunnel is negligible.

Bubbles can be implanted in airstreams of 200 fps or higher at extremely rapid production rates. However, good photography of the bubble traces is presently limited to about 100 fps in a large-scale wind tunnel. More intense lighting and/or better bubble reflectivity are needed for photography at higher airspeeds.

Still streak photography has been thoroughly developed and proven. In addition, limited results from motion and stereo photography, as well as video tape, are quite encouraging. These latter techniques will be especially valuable in studying unsteady and highly three-dimensional flow patterns. Consequently, it is recommended that more work be carried out along these lines.

Flow tracing accuracy is excellent within the existing range of airspeeds of the system, as long as the aerodynamic model is not too small. To assess properly any accuracy limitations at higher airspeeds, more information is required about the drag force on an accelerating bubble. At the same time, an effort should be made to establish the Stokes number, or an alternative parameter, as a valid correlation parameter for flow tracing accuracy.

The visualizations of the tip vortex obtained during this investigation provide new insight into this phenomenon. Particularly significant is the rapid entrainment of the airflow about the blade tip into the vortex core and the continuing radial inflow downstream.

REFERENCES

1. Hale, R. W., Tan, P. and Ordway, D. E., Experimental Investigation of Several Neutrally-Buoyant Bubble Generators for Aerodynamic Flow Visualization, Sage Action, Inc., SAI-RR 6901, August 1969; AD-717 390.

2. Mysels, K. J., Soap Films and Some Problems in Surface and Colloid Chemistry, The Journal of Physical Chemistry, Vol. 68, No. 12, pp. 3441-3448, December 15, 1964.

3. Boys, C. V., Soap Bubbles, Their Colours and the Forces Which Mold Them, Dover Publications, Inc., New York, 1959.

4. Kuehner, A. L., New Tough Films and Bubbles, Journal of Chemical Education, Vol. 25, pp. 211-212, April 1948.

5. Kuehner, A. L., Long-Lived Soap Bubbles, Journal of Chemical Education, Vol. 35, No. 7, pp. 337-338, July 1958.

6. Stong, C. L., The Amateur Scientist, Scientific American, Vol. 220, No. 5, pp. 128-134, May 1969.

7. Lock, C. N. H., Photographs of Streamers Illustrating the Flow Around an Airscrew in the "Vortex Ring State", ARC Reports and Memoranda No. 1167, April 1928.

8. Redon, M. H. and Vinsonneau, M. F., Étude de l'Écoulement de l'Air Autour d'une Maquette, L'Aéronautique, Bulletin "L'Aérotechnique", Vol. 18, No. 204, pp. 60-66, May 1936.

9. Redon, H., Means for Materializing the Streamlines of a Fluid, United States Patent Office, Patent No. 2,134,890, November 1, 1938.

10. Kampé de Fériet, J., Some Recent Researches on Turbulence, Proceedings of the Fifth International Congress for Applied Mechanics, Cambridge, Massachusetts, September 12-16, 1938, pp. 352-355, John Wiley & Sons, Inc., New York, 1939.

11. Owen, F. S., Hale, R. W., Johnson, B. V. and Travers, A., Experimental Investigation of Characteristics of Confined Jet-Driven Vortex Flows, United Aircraft Research Laboratories, Report R-2494-2, November 1961; AD-328 502.

12. Rinehart, S. A., Balcerak, J. C. and White, R. P., Jr., An Experimental Study of Tip Vortex Modification by Mass Flow Injection, Rochester Applied Science Associates, Inc., Report 71-01, January 1971; AD-726 736.

13. ———, SAI Bubble Generator, Model 3, Sage Action, Inc., Ithaca, New York, January 1971. Available from Sage Action, Inc.

14. Taylor, M. F. and Masser, C. C., Photographic Study of a Bromine Jet in a Coaxial Airstream, NASA TN D-4660, 1968.

15. Masser, C. C. and Taylor, M. F., Photographic Study of a Bromine Jet Flowing in a Coaxial Airstream and Impinging on a Stagnation Surface, NASA TN D-5209, 1969.

16. ———, Kodak Professional Black-and-White Films, Kodak Publication No. F-5, Eastman Kodak Company, Rochester, New York, 1969. Available from Eastman Kodak Company.

17. ———, Kodak 2475 Recording Film (ESTAR-AH Base), Kodak Pamphlet No. P-95, Eastman Kodak Company, Rochester, New York, 1968. Available from Eastman

Kodak Company.

18. Fuchs, N. A., The Mechanics of Aerosols, Pergamon Press and The Macmillan Company, New York, 1964.

19. Odar, F. and Hamilton, W. S., Forces on a Sphere Accelerating in a Viscous Fluid, Journal of Fluid Mechanics, Vol. 18, Part 2, pp. 302-314, February 1964.

20. Robinson, B. R., The Acceleration of Neutrally Buoyant Spheres in a Uniform Flowing Fluid, National Aeronautical Establishment, National Research Council of Canada, Report LTR-LA-43, October 1969.

21. Chigier, N. A. and Corsiglia, V. R., Tip Vortices - Velocity Distributions, 27th Annual National Forum of the American Helicopter Society, Washington, D. C., Preprint No. 522, May 19-21, 1971.

22. McCormick, B. W., Aircraft Wakes: A Survey of the Problem, FAA Symposium on Turbulence, Washington, D. C., March 22-24, 1971.